DEVELOPMENT OF THIN FILM GAAS P-I-N SOLAR CELLS PEELED-OFF FROM SI SUBSTRATES

Furkan AZİM

Master's Thesis

Department of Physics

Programme in Solid State Physics

Supervisor: Assoc. Prof. Dr. Mustafa KULAKCI

Eskişehir

Eskişehir Technical University

Institute of Graduate Programs

March 2022

This study was supported in part by The Scientific and Technological Research Council of Turkey (TUBITAK) under the Grant No. 118M055 and 120F222.

11/03/2022

SUPERVISOR APPROVAL

Master's student Furkan AZİM, whom I supervise, has completed this thesis titled DEVELOPMENT OF THIN FILM GAAS P-I-N SOLAR CELLS PEELED-OFF FROM SI SUBSTRATES. According to my inspections, the work is scientifically and ethically appropriate for the student to the thesis defense exam.

Supervisor

Assoc. Prof. Dr. Mustafa KULAKCI

ABSTRACT

DEVELOPMENT OF THIN FILM GAAS P-I-N SOLAR CELLS PEELED-OFF FROM SI SUBSTRATES

Furkan AZİM

Department of Physics

Programme in Solid State Physics

Eskişehir Technical University, Institute of Graduate Programs, March 2022

Supervisor: Assoc. Prof. Dr. Mustafa KULAKCI

III-V group semiconductor solar cells are the most efficient photovoltaic technologies. In particular, III-V group based GaAs solar cells provide excellent optical properties, good electronic speed, and higher radiation resistance over conventional Si solar cells. However, the high prices of single crystal III-V based wafers restrict the use of GaAs in photovoltaic applications. As a result, cost-cutting approaches for III-V solar cells have piqued the interest of many researchers. The epitaxial lift-off (ELO) method has been receiving much interest for producing flexible, lightweight, and high-efficient solar cells. The method also allows for the reuse of pricey III-V substrates for subsequent growths, reducing overall cost. Heteroepitaxial growth of III-V semiconductors on low-cost Si substrates, on the other hand, is another method for reducing the cost of GaAs solar cells. Using Si substrates also allows for large-scale production of III-V solar cells. In this thesis, GaAs solar cells were grown on Si substrates using a molecular beam epitaxy (MBE) system. GaAs solar cells were designed as p-i-n type junctions to improve charge extraction. The effects of various types of dislocation filter approaches were compared to achieve the best crystal quality. Before and after the ELO process, optical and structural characterizations of solar cell structures were performed. The energy conversion and quantum efficiency values of the solar cell were measured. Thin-film GaAs p-i-n solar cells peeled off from Si substrates have achieved 8.81% energy conversion efficiency under the 1.5AMG spectrum.

Keywords: GaAs, Epitaxial lift-off, Flexible thin-film solar cell, Photovoltaics.

ÖZET

P-İ-N YAPIDA GAAS TABANLI ESNEK İNCE FİLM GÜNEŞ HÜCRELERİNİN Sİ ALTTAŞLAR ÜZERİNDEN GELİŞTİRİLMESİ

Furkan AZİM

Fizik Anabilim Dalı

Katıhal Fiziği Bilim Dalı

Eskişehir Teknik Üniversitesi, Lisansüstü Eğitim Enstitüsü, Mart 2022

Danışman: Doç. Dr. Mustafa KULAKCI

III-V grubu yarı iletken güneş hücreleri en verimli fotovoltaik teknolojilerdir. Özellikle III-V grubu tabanlı GaAs güneş hücreleri, geleneksel Si güneş hücrelerine göre mükemmel optik özellikler, daha iyi elektronik hız ve daha yüksek radyasyon direnci sağlar. Bununla birlikte, tek kristal III-V tabanlı alttaşların yüksek fiyatları, fotovoltaik uygulamalarda GaAs malzemelerin kullanımını kısıtlamaktadır. Sonuç olarak, III-V güneş hücreleri için maliyet düşürme yaklaşımları birçok araştırmacının ilgisini çekmiştir. Epitaksiyel kaldırma (ELO) yöntemi; esnek, hafif ve yüksek verimli güneş hücreleri üretimi için büyük ilgi görmektedir. Yöntem ayrıca yüksek maliyetli III-V alttaşların sonraki büyütmeler için yeniden kullanılmasına izin vererek toplam maliyeti düşürür. III-V yarı iletkenlerinin düşük maliyetli Si alttaşlar üzerinde heteroepitaksiyel büyütülmesi ise diğer bir GaAs güneş hücrelerinin maliyetini düşürme yöntemidir. Si alttaşların kullanılması aynı zamanda III-V güneş hücrelerinin büyük ölçekli üretimine de olanak tanır. Bu tezde GaAs güneş hücreleri, moleküler ışın epitaksi (MBE) sistemi kullanılarak Si alttaşlar üzerine büyütülmüştür. GaAs güneş hücreleri, yük ekstraksiyonunu iyileştirmek için p-i-n tipi eklem olarak tasarlanmıştır. En iyi kristal kalitesini elde edebilmek için çeşitli dislokasyon filtre yaklaşımları kullanılmış ve etkileri karşılaştırılmıştır. ELO işleminden önce ve sonra güneş hücrelerinin optik ve yapısal karakterizasyonları yapılmıştır. Güneş hücrelerinin enerji dönüşümü ve kuantum verim değerleri ölçülmüştür. Si alttaşlardan kaldırılmış ince film GaAs p-i-n güneş hücreleri, 1.5AMG spektrumu altında %8.81 enerji dönüşüm verimliliği elde etmiştir.

Anahtar Sözcükler: GaAs, Epitaksiyel film kaldırma, Esnek ince film güneş hücresi, Fotovoltaik

ACKNOWLEDGEMENTS

I would like to express my sincere gratitude to Assoc. Prof. Dr. Mustafa Kulakcı for his support and guidance during my study. I would also like to thank Prof. Dr. Uğur Serincan for his support.

I would like to thank all members of the Nanoboyut Research Laboratory; Assist. Prof. Dr. Burcu Arpapay, Onur Şenel, Ali Büyükpınar, Elif Yılmaz and Ayşe Aygül Yılmaz Ergürhan, for their valuable contributions and help.

Finally, I would like to thank Cansel Paluli and my family for their patience, support, and love.

Furkan AZİM

11/03/2022

STATEMENT OF COMPLIANCE WITH ETHICAL PRINCIPLES AND RULES

I hereby truthfully declare that this thesis is an original work prepared by me; that I have behaved in accordance with the scientific ethical principles and rules throughout the stages of preparation, data collection, analysis and presentation of my work; that I have cited the sources of all the data and information that could be obtained within the scope of this study, and included these sources in the references section; and that this study has been scanned for plagiarism with "scientific plagiarism detection program" used by Eskişehir Technical University, and that "it does not have any plagiarism" whatsoever. I also declare that, if a case contrary to my declaration is detected in my work at any time, I hereby express my consent to all the ethical and legal consequences that are involved.

Furkan AZİM

CONTENTS

Page

LIST OF TABLES

Page

LIST OF FIGURES

Page

LIST OF IMAGES

Page

GLOSSARY OF SYMBOLS AND ABBREVIATIONS

Å	:	Angstrom
°C	:	Celsius
η	:	Conversion efficiency
ω	:	Omega
θ	:	Theta
λ	:	Wavelength
μm	:	Micrometer
Al	:	Aluminium
AlAs	:	Aluminium arsenide
AM	:	Air mass
APD	:	Anti-phase domain
ARC	:	Anti-reflection coating
APB	:	Anti-phase boundary
arcsec	:	Arcsecond
As	:	Arsenic
Au	:	Gold
CLEFT	:	Cleavage of lateral epitaxial films for transfer
cm	:	Centimeter
CMP	:	Chemo-mechanical polishing
CPV	:	Concentrator photovoltaic
$C_6H_8O_7$	:	Citric acid
DI	:	Deionised
ELO	:	Epitaxial lift-off
eV	:	Electronvolt
EQE	:	External quantum efficiency
E_V	:	Valance band
E_C	:	Conduction band
FF	:	Fill factor
FWHM	:	Full-width-at-half-maximum
g	:	Gram

Ga	:	Gallium
GaAs	:	Gallium arsenide
h	:	Planck constant
HALE	:	High altitude long endurance
HCl	:	Hydrochloric acid
HELO	:	Heteroepitaxial lift-off
HF	:	Hydrofluoric acid
HRXRD	:	High-resolution X-ray diffraction
H_2O	:	Water
H_2O_2	:	Hydrogen peroxide
In	:	Indium
InAs	:	Indium arsenide
IQE	:	Internal quantum efficiency
I_{sc}	:	Short-circuit current
J_{sc}	:	Short-circuit current density
K	:	Kelvin
kg	:	Kilogram
m	:	Meter
mA	:	Milliampere
MBE	:	Molecular beam epitaxy
MgF_2	:	Magnesium fluoride
MJ	:	Multi-junction
MPa	:	Megapascal
N_2	:	Nitrogen
Ni	:	Nickel
nm	:	Nanometer
NREL	:	National renewable energy laboratory
P	:	Phosphorus
PCE	:	Power conversion efficiency
P_{in}	:	Input power
PV	:	Photovoltaic
PL	:	Photoluminescence

Pt	:	Platinum
PVD	:	Physical vapour deposition
QE	:	Quantum efficiency
RHEED	:	Reflection high-energy electron diffraction
Si	:	Silicon
SEM	:	Scanning electron microscope
SLS	:	Strain layer superlattice
SQ	:	Shockley – Queisser
T	:	Temperature
Ti	:	Titanium
TCA	:	Thermal cycle annealing
UAS	:	Unmanned aircraft system
UHV	:	Ultra-high vacuum
UV	:	Ultraviolet
V	:	Volt
V_{oc}	:	Open-circuit voltage
W	:	Watt
WI – ELO	:	Weight-induced epitaxial lift-off
ZnS	:	Zinc sulfide

1. INTRODUCTION

Energy is required for our existence. Fossil fuels have long been the preferred choice for obtaining the energy we require to live and advance our civilization. However, due to dependence on fossil fuels, climate change has begun to harm our environment and has generated dramatic natural phenomena all over the planet [1]. As a consequence, researchers are paying close attention to renewable energy production. Among renewable energy production technologies, solar power has the greatest potential to be the first choice against fossil-based energy. Photovoltaics (PV) is the rapidly growing solar-fueled and carbon-free energy technology. As a result of gaining attraction to the PV systems, the photovoltaic market has increased and the price of PV arrays has fallen consistently during the last few decades. Despite these developments in PV technology, they remain reliant on subsidies, mainly government programs. Existing PV technologies must be more efficient and cheaper to be widely used in order to broad usage.

Currently, silicon solar cells are the market leader in PV systems because they are relatively inexpensive, non-toxic, reliable, and mature technology. However, silicon has some disadvantages that reduce solar cell performance and makes it a poor choice for optoelectronic applications. Silicon is an indirect bandgap material with a low ability to absorb incident light and, to realize high efficiencies, thick and high-purity silicon wafers are needed. As a result, the cells become heavier and the costs increase. Plus, silicon isn't a good material for the space environment due to its poor radiation resistance. Alternative technologies have been studied for decades and among all the other PV technologies, III-V group solar cells are the first choice over silicon counterparts in order to realize high efficiency.

The III-V group solar cells have superior properties and are excellent candidates for achieving maximum PV conversion efficiency. They have a direct bandgap with high absorption coefficients, radiation resistance, and potential usage in multi-junction applications. Gallium Arsenide (GaAs) solar cells, in particular, have the highest power conversion efficiency (PCE) of 29.1% for single-crystal solar cells so far [2]. GaAs is the most suitable material for space applications as well, due to their strong light absorption properties and radiation resistance. However, GaAs is a far more expensive material than silicon and this limits their range of uses. GaAs solar cells must be more affordable and

efficient to overcome this limited range of applications. There are various approaches to reduce the cost of solar cells. In this study, two of them are used.

First, the integration of GaAs and Si offers a great deal of cost reduction. The majority of the cost of a GaAs solar cell comes from the wafer, which comprises about %90 of the cell cost [3] and, substituting GaAs wafers with relatively inexpensive Si wafers lowers the total cost. Furthermore, silicon technology is matured as a consequence of the microelectronics industry so that it is readily available in large Si wafer sizes compared to GaAs wafers, which leads to additional cost savings. The development of GaAs on Si wafers has long been of interest in order to enjoy the benefits of both materials, and the approach has achieved an efficiency of %20 [4].

Second, separating the active layer from its wafer and reusing the separated wafer many times after cleaning processes reduces the cost even further. Although Si wafers are significantly cheaper than GaAs wafers, they are still expensive to manufacture and contribute to most of the overall cost of the solar cell. Since GaAs is a semiconductor with a direct bandgap, even a thin layer of GaAs is enough to absorb the incident light without loss. Epitaxial Lift-Off (ELO) is a technique that is used to separate III-V solar cells from their underlying substrate and allows the reuse of the substrate after the cleaning processes. After the separation process, the separated solar cell layer can be transferred onto low-cost carriers. Thin-film solar cells also have the advantage of being lightweight and flexible, which is very important for aerospace applications.

In this thesis, GaAs solar cells are grown onto Si substrates and then the ELO technique is utilized to separate the active GaAs layer. Polyamide is used as a carrier of separated thin GaAs solar cells. Thin-film GaAs solar cells separated from Si substrates have been found to exhibit an efficiency comparable to thin-film GaAs solar cells separated from GaAs substrates as reference cells. The possibility of thin-film III-V solar cells separated from Si substrates is shown by this study.

1.1. Organization of Work

This thesis consists of the following chapters:

Chapter 2 presents the III-V solar cells and their properties, the ELO process, and the III-V/Si integration.

Chapter 3 presents the basic concepts and the working principles of a solar cell, descriptions of solar cell parameters.

Chapter 4 consists of fabrication and characterization methods and all production steps used throughout the thesis.

Chapter 5 includes the characterization of devices and the discussion of device performance results.

Chapter 6 includes a summary of the study and a conclusion of the thesis study.

2. III-V SOLAR CELLS

III-V group semiconductors are alloys made up of elements from the periodic table groups III (Ga, In, Al) and V (N, As, P, As). They are bonded primarily by covalent bonding and the majority of them have a zinc-blende crystal structure and direct bandgap. Aside from having excellent optical and electrical characteristics, compound III-V group semiconductors can be formed into binary (GaAs etc.), ternary (AlGaAs etc.), quaternary (AlGaAsP etc.), or more complex structures and widely used in multi-junction (MJ) applications. The energy bandgap can be adjusted to match the highest performance of the targeted device depending on the combination of elements in the alloy. These superior properties over elemental semiconductors enable a wide range of applications, including solar cells, LEDs, photodetectors, LASERs, and high-frequency electronics. Particularly, III-V group solar cells have proved their capability in solar cell applications with the best power conversion efficiencies and are the best choice for high-efficiency applications.

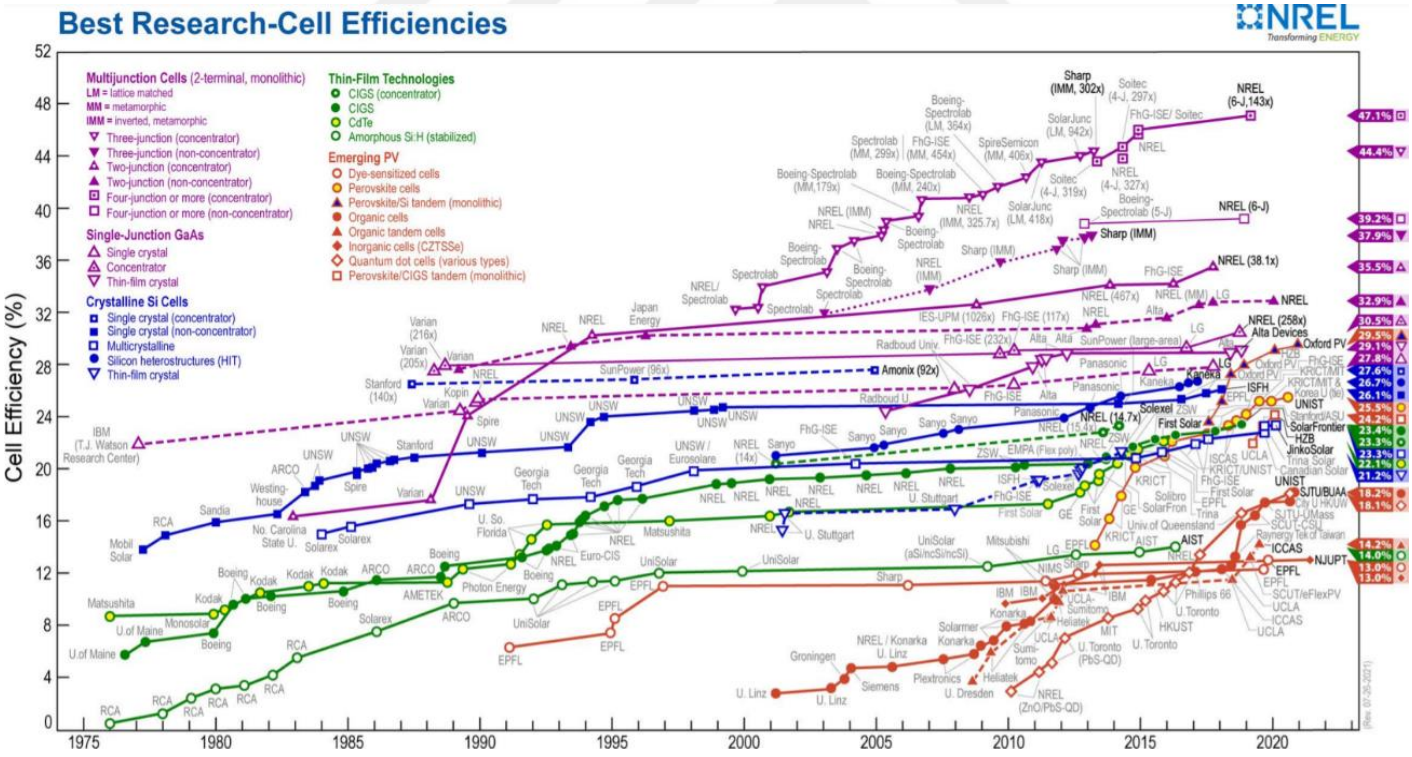

Figure 2.1. *Various PV technologies and their change of power conversion efficiencies over years. Purple color represents III-V solar cell technologies [2]*

2.1. GaAs

GaAs is the most understood and widely used member of the III-V semiconductor family. GaAs is a zinc-blende structured compound in which each gallium (Ga) atom is bonded to four neighboring arsenic (As) atoms as seen in Figure 2.2. Here, “a” stands for lattice constant and is 5.65325Å at room temperature.

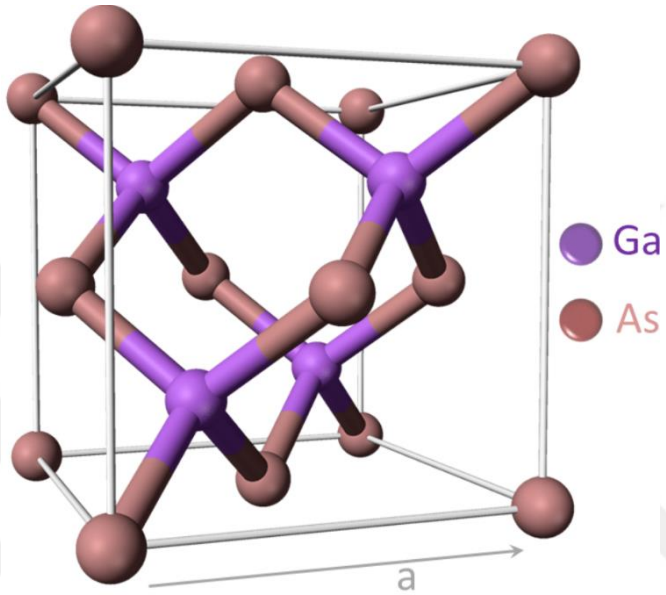

Figure 2.2. *Zinc-blende structure of GaAs*

With an energy bandgap of 1.42 eV, GaAs is close to the optimal value for the standard solar spectrum, allowing for theoretically maximum conversion efficiency of 31% for single-junction solar cells [5]. Currently, GaAs has reached the power conversion efficiency of 29.1% by ALTA Devices Inc. and hold the title of being the highest efficiency for single-junction solar cells [6]. GaAs, like many other III-V semiconductors, has a direct bandgap and strongly absorb the incident light. Over visible wavelengths, the absorption coefficient of GaAs is about ten times higher than the absorption coefficient of silicon. It thus allows the thickness of GaAs solar cells to be reduced. The ability to make thinner solar cells is critical for space applications where weight is a concern. Also by less expensive GaAs material is used, the cost is reduced.

There are additional benefits of using GaAs as a solar cell. One is a good temperature coefficient. Solar cell efficiency tends to decrease as temperature rises. GaAs solar cells operate better in high-temperature environments than silicon due to this temperature coefficient. Also, GaAs and other III-V materials have high electron mobility so that created electrons can be effectively converted into electricity. Finally, GaAs is inherently resistant to degradation from moisture and radiation, which is also important for aerospace applications. Some of the properties of GaAs are listed in Table 2.1.

Table 2.1 *Selected important properties of GaAs at 300 K [7]*

Lattice constant (Å)	5.653
Density (g/cm^3)	5.318
Band-gap energy (eV)	1.424
Band-gap type	Direct
Electron mobility (cm^2/Vs)	8500
Hole mobility (cm^2/Vs)	400
Intrinsic carrier concentration (cm^{-3})	1.84 x 10^6

The major drawback of III-V solar cells has always been their high cost. The cost of III-V solar modules is approximately 400 times that of mainstream silicon solar modules, which limits their application range [8]. In order to increase the market demand for III-V solar cells, the costs must be reduced. One way to reduce the III-V solar cell cost is to make a thin-film structure and to reuse the substrate several times.

2.2. Thin Film III-V Solar Cells

III-V thin-film solar cell technology is attractive for researchers not only because of its low cost, but also because of its lower weight, improved performance, and structural flexibility. III-V solar cells are generally produced on expensive germanium (Ge) or GaAs substrates, which contribute most of the overall price and make the cell thick. III-V semiconductors have excellent optical properties and can easily be formed in a thin-film structure without efficiency loss. There are also other benefits of thin-film solar cells. Thin-film III-V solar cells have higher radiation hardness than wafer-based III-V solar cells, which is preferable for harsh environment applications. Solar cells that are

lightweight and flexible are also essential for space missions where high specific power conversion (W/kg) is required. Furthermore, thin-film III-V solar cells take advantage of the photon recycling effect and outperform the substrate-based equivalents in terms of power conversion efficiency [9, 10].

2.2.1. Epitaxial Lift-Off

There are several methods to produce thin-film III-V cells such as epitaxial lift-off (ELO) [11], controlled spalling technology [12], cleavage of lateral epitaxial films for transfer (CLEFT) [13], and exfoliation [14]. Among these, the ELO technique is the most mature and offers the most potential for cost reduction due to minimal harm to the substrate and the possibility to reuse the substrate several times. The ELO method uses selective wet etching to separate an active thin-film layer from its substrate. This is performed by forming a thin sacrificial $Al_xGa_{1-x}As$ (x>0.6) layer between the active thin-film layer and the substrate and etching it with an aqueous hydrofluoric acid (HF) solution. The separated thin-film device layer then can be transferred to a low-cost carrier material such as glass or polyamide. The photon recycling effect is utilized because the back contact acts as a mirror and increases the optical path of a photon within the solar cell, leading the thin-film solar cells to perform better than substrate-based solar cells. Following the chemo-mechanical polishing (CMP) processes to remove the sacrificial layer residues, the substrate can be reused for new solar cells. In Figure 2.3, a comparison of standard substrate-based solar cell processes and thin-film solar cell processes are shown.

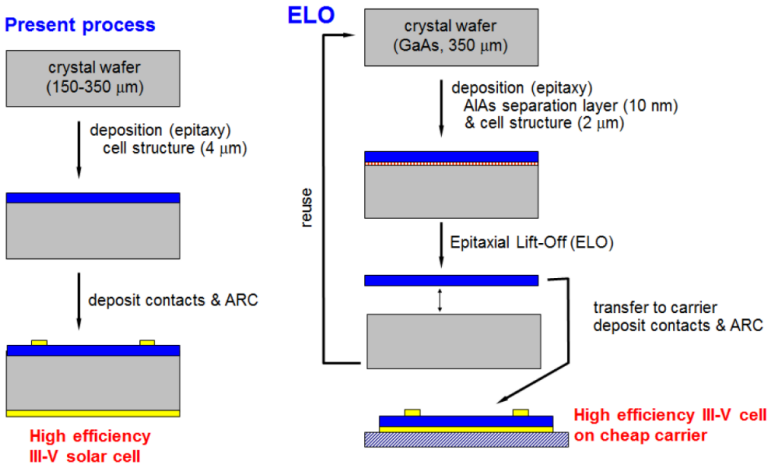

Figure 2.3. *A comparison of substrate-based solar cell processes and ELO solar cells processes [15]*

In 1978 Konagi et al. were the first to propose the ELO technique as “peeled film technology”, which uses selective etching to separate GaAs solar cells from their underlying GaAs substrate [16]. Although Konagi et al. were successful in demonstrating thin-film GaAs solar cells with this study, the process was unsuitable for practical use because etching the sacrificial layer was too slow.

Yablonovitch et al. enhanced the peeled film technology in 1987 to create thin-film GaAs layers [17]. The study involved utilizing a sufficiently thin sacrificial layer to effectively curl the thin-film active layer and transferring the thin-film active layer to another carrier using black wax as a handle. The wax-induced compressive strain in the layer causes the thin film to curl during etching and keeps the gap between the thin layer and substrate open, allowing the etchant solution to access more easily to the sacrificial layer. The process was renamed the "epitaxial-lift off" later on. However, further improvements were required before the method could be implemented on an industrial basis. The etching speed was still slow, and only a few millimeter-sized devices could be produced. Furthermore, the strain induced by the wax was difficult to control, making it difficult to optimize the process to speed it up.

During the mid-1990s, researchers focused on improving the method in order to overcome the technique's drawbacks. The parameters that influence the etching time have been thoroughly investigated. In addition, some changes are made to the original ELO approach. Schermer et al. achieved an etching rate of more than 10mm/hr utilizing their weight-induced epitaxial lift-off (WI-ELO) technique [18]. Using the WI-ELO technique, Schermer et al. reached a very high power conversion efficiency of 26.1% for single-junction thin-film GaAs solar cells in 2009 [19].

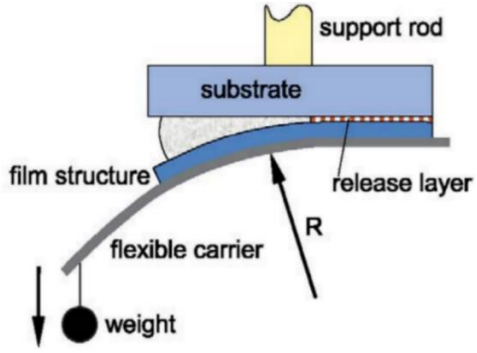

Figure 2.4. *Schematic of WI-ELO method [20]*

The WI-ELO method has the problem of cracking the thin films at the end of the lifting process due to extreme bending generated by their own weight. One of the solutions is to maintain a constant radius of bending curvature. To resolve this problem, the advanced WI-ELO method was developed. Instead of using weight through the flexible carrier, which results in a variable radius, the advanced WI-ELO approach utilizes a guiding cylinder to maintain the radius constant as shown in Figure 2.5. With the advanced WI-ELO method, an etching rate of more than 30 mm/h is achievable without any cracks on the films [20].

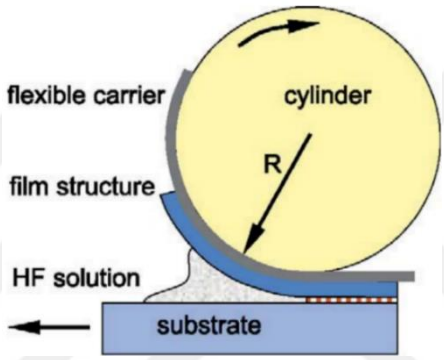

Figure 2.5. *Advanced WI-ELO [20]*

2.2.2. Applications of Thin-Film III-V Solar Cells

Thin-film III-V solar cells not only have a high PCE, but are also lightweight, flexible, have high radiation endurance, and have good thermal behavior. These advantages, together with the fact that III-V group semiconductors are the most efficient solar cell materials, make III-V solar cells the ideal choice for space applications that operate in harsh environments. Currently, the majority of solar cells used in space are wafer-based III-V MJs on Ge cells because of their high power conversion efficiency and radiation endurance. They are placed atop a rigid honeycomb structure to protect the wafers from damage, which results in higher weight. Thin-film solar cells eliminate the need for these structures, this paves the path for new low-weight panel designs. Also, thin-film III-V solar cells have the benefit of being able to be folded and rolled. Both InSight and Phoenix Mars landers, for example, employed Next Generation UltraFlex blanket flexible solar arrays for this purpose.

III-V thin-film solar cells have great potential for clean technologies and are ideal for use in electrical vehicles such as aircraft and electric cars. Their high power output and lightweight characteristics are suitable for these applications. Solar Impulse 2, a solar aircraft, used 17.000 Si-based solar cells to achieve the longest solo flight without fuel. If the solar cells were thin-film III-V solar cells, it would require fewer solar cells, resulting in a lighter weight and higher energy. Thin-film III-V solar cells will be able to replace silicon solar cells in such applications in the future, opening up new markets.

Portable electric charges and unmanned aerial vehicles (UAVs) are two additional important applications for flexible and lightweight thin-film solar cells. For military applications requiring a portable charging station, a 10.25x15.5 inch panel with 30 single-junction thin-film GaAs solar cells has been developed [21] and used in military applications. Thin-film solar cells also have desirable features for UAV applications, such as high power conversion efficiency and high W/kg. Image 2.1 (d) and (e) shows two MicroLink UAV prototypes. The Raven UAV and Puma UAV are small UAVs that use MicroLink's ELO triple-junction solar cell technology [22]. In Image 2.1, Phoenix Mars lander (a), Solar Impulse 2 (b), and portable charging station for military purposes (c) are also shown.

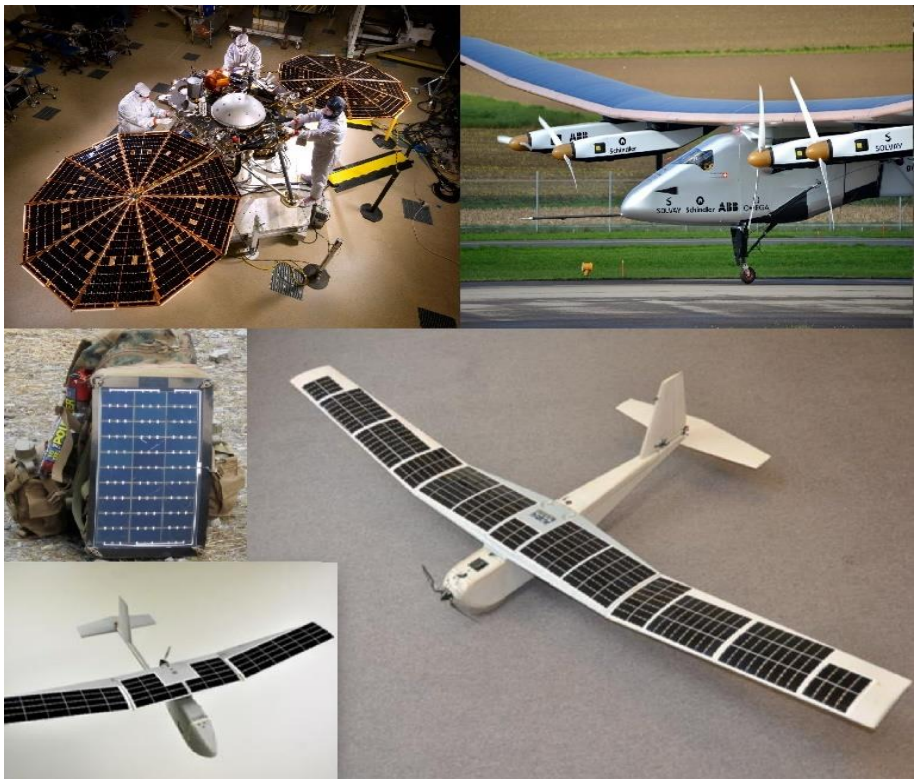

Image 2.1. *Mars lander [23], Solar Impulse 2 [24], mobile charge station [21], UAVs [22]*

Thin-film III-V solar cells are less expensive than wafer-based III-V solar cells, however, they are still prohibitively expensive for terrestrial applications. Because of the substrate preparation processes for new growth, extensive reuse of the substrate does not reduce the high cost of III-V substrates sufficiently (Figure 2.6). To increase market demand from terrestrial applications, costs must be reduced further and power conversion efficiency must be increased. Concentrator PV (CPV) systems are one way to employ high-efficiency thin-film III-V solar cells in terrestrial applications. Thin-film III-V solar cells powered by CPV can be placed on an apartment or building rooftops, as well as charge stations for electric cars. Thin-film III-V solar cells can also be used in agricultural technology applications and large-scale PV power facilities. Another strategy to cut prices and increase demand for III-V solar cells is to combine the high-efficiency III-V active layer with inexpensive and advanced technology-based substrates like silicon.

Reuse strategy	10 times	20 times	50 times	100 times
ELO with CMP every cycle	$34 ($32)	$26 ($24)	$21 ($18)	$19 ($17)
ELO with CMP every 10 cycles	$24 ($22)	$16 ($13)	$11 ($8)	$9 ($7)

Figure 2.6. *Table of the cost per cell as a function of substrate reuse cycles for the ELO technique. The values in parentheses indicate the cost per cell if the epitaxial deposition costs are reduced in the future [3]*

2.3. III-V Solar Cells on Silicon

For the past several decades, researchers from all around the world have been attracted to the integration of III-V semiconductors with silicon technology. A significant amount of work and money is spent to integrate the advantages of both materials. Especially for solar cells, the fundamental driving factor was the replacement of expensive III-V substrates with inexpensive silicon substrates and reaching high volume manufacturing throughput of the silicon technology.

III-V semiconductors are well-known for their superior optical properties, having a direct bandgap, high absorption coefficient across the visible region of the spectrum and excellent electronic quality makes them unrivaled for high-efficiency required applications. However, they are also well-known for their high price. On the other hand, silicon technologies have matured with the massive microelectronic and photovoltaic

industry, and silicon wafers are available in larger diameters than Ge, GaAs, or InP wafers. Integrating III-V semiconductors with this advanced silicon technology would increase the volume of III-V solar cell production and decrease the cost further.

There are additional benefits of integrating III-Vs on silicon substrates. Compared to III-Vs, silicon semiconductors offer superior mechanical and thermal characteristics. Silicon is a better material with high thermal conductivity for high-temperature applications, such as concentrator systems, where excess heat must be removed from the solar cell. Transferring heat out of the solar cell through the silicon substrate, which has approximately 2x higher thermal conductivity than GaAs and Ge substrates, will prevent the lower power conversion efficiency.

Mechanical strength is another benefit of employing silicon substrates. Having a higher fracture toughness value than GaAs and Ge makes the silicon mechanically stronger. This characteristic enables for not only mechanically stronger but also lighter solar cells. Using thinner silicon substrates reduces cost and mass without losing mechanical strength. Furthermore, silicon has a lower mass density than GaAs and Ge, allowing for an even greater mass reduction in silicon-based substrate solar cells. The use of lighter solar cells is required in applications such as space-based PV systems or rooftop PV systems where mass is an important factor. In addition, specific power (W/kg) will increase with such lighter solar cells. Table 2.2 illustrates a comparison of some properties of Si, GaAs, and Ge.

Table 2.1. *Selected properties of Si, GaAs, Ge and their comparison [25]*

Substrate Qualities	GaAs	Ge	Si
Mass density (g.cm^{-3})	5.316	5.323	2.329
Fracture toughness (MPa.$m^{1/2}$)	0.4-0.5	~0.6	~0.9
Thermal conductivity (W. $cm^{-1}.K^{-1}$)	0.56	0.64	1.24
Thermal expansion mismatch (versus GaAs)	0%	0%-3%	70%-120%
Lattice mismatch (versus GaAs)	0%	0.08%	4.1%

However, integrating III-V and silicon is difficult due to various mismatches between them. These mismatches cause defects and microcracks as the III-V layer grows over silicon substrate, resulting in significant efficiency loss in solar cell performance.

The most serious issues include lattice mismatch, crystal symmetry mismatch, and differences in thermal expansion coefficients.

4.1% lattice mismatch between GaAs and silicon causes misfits and threading dislocation densities (TDDs) in the GaAs film during growth due to increased strain energy. Dislocations are overcome by developing substrate engineering, buffer layer technologies, and thermal annealing techniques [26-28].

Silicon and GaAs have different crystal symmetries. Because silicon is a monoatomic semiconductor and GaAs is a diatomic semiconductor, silicon has non-polar nature while GaAs have polar nature. Antiphase Boundaries (APBs) are introduced during the growth of polar GaAs on non-polar silicon. Offcut silicon substrates with angles ranging from 2° to 7° can be employed to reduce APBs in the device [26-28].

The large difference in thermal expansion coefficient between GaAs and silicon induces thermal cracks in the device as a result of introduced thermal strain during the temperature change. The solutions for dealing with thermal cracks in the device include growing a layer that is less thick than the critical cracking thickness, using buffer layers, and using patterned substrates [26-28].

Space applications are the major reason for employing III-V/Si solar cells. The high efficiency and radiation endurance of III-Vs, combined with the superb physical properties and lightness of silicon, provide enormous potential for space solar cells. Yamaguchi et al. achieved the highest ever reported GaAs/Si solar cell efficiency of 18.3% at AM0 and 20% at AM1.5 [4]. They also discovered that GaAs/Si solar cells performed better in terms of end-of-life efficiency and radiation endurance than GaAs/GaAs solar cells. These findings indicate a high potential for employing GaAs/Si solar cells in future aerospace missions.

3. BASIC CONCEPTS OF PHOTOVOLTAICS

3.1. Solar Irradiation

The sun generates a massive amount of energy, around 64 MW/m^2 on its surface. The temperature is around 6000 K at the surface, and the sun's spectrum behaves similar to that of a blackbody. The total solar irradiation is reduced to about 1367 W/m^2 after traveling roughly 1.5x10^{11} meters from the Sun to the Earth. Incident light is absorbed, reflected, and scattered through the atmosphere, which contains various atoms and molecules. Figure 3.1 shows the final solar spectrum that reaches Earth's surface, AM0 and AM1.5G radiation.

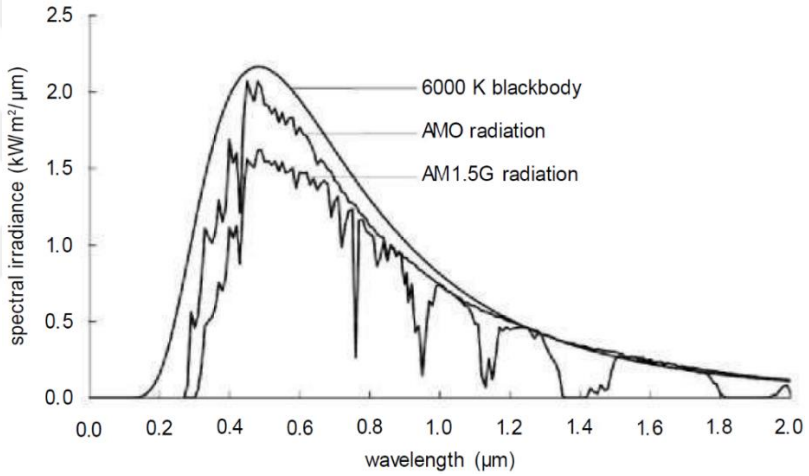

Figure 3.1. *Solar irradiation at AM0 and AM1.5G [29]*

The Air Mass (AM) is a measure of the reduction in light power and is defined as follows;

$$AM = \frac{1}{cos\theta} \tag{3.1}$$

where θ is the zenith angle, which is the angle between the sun and its vertical axis, as illustrated in Figure 3.2. AM0 represents the radiation just outside the atmosphere, and this spectrum is used for space applications. AM1 spectrum is when the sun is at the vertical direction, and AM1.5 spectrum is when the sun is at 48.2° zenith angle. The AM1.5 spectrum is used as a standard in terrestrial applications. The AM1.5 can be further divided into AM1.5G (global) and AM1.5D (direct) radiation, where scattering

and reflection effects in the atmosphere are taken into account. In AM1.5G, these effects are included in solar radiation, whereas in AM1.5D, they are not.

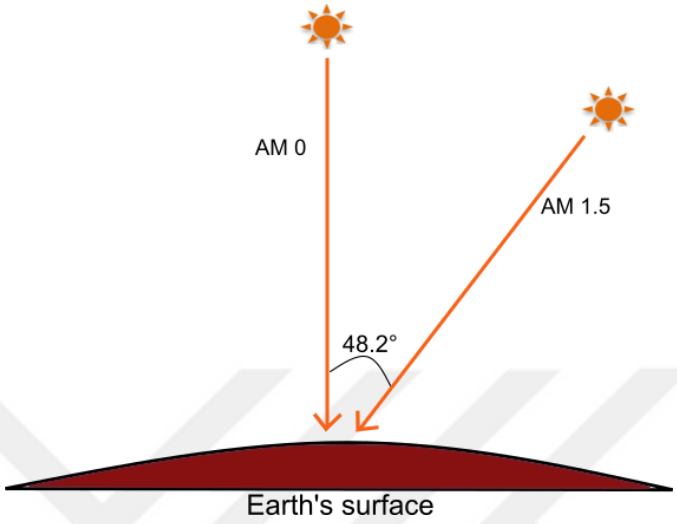

Figure 3.2. *Illustration of AM0 and AM1.5 spectrums*

3.2. Basic of Solar Cells

Solar cells are electronic devices that operate similarly to diodes. They produce electricity by converting incident light. Most of them are in the form of the p-n junction, but there are other types as well, such as p-i-n or Schottky junctions. The photovoltaic effect, which is closely related to the photoelectric effect, lies at the heart of solar cell operation. In the photoelectric effect, a photon with energy equal to or higher than the specific energy of metal is absorbed by the metal, causing electrons to be emitted. This specific energy is the minimum required energy to eject the electron from the metal and is called the work function. The kinetic energy of the emitted electrons is given as;

$$KE = h\nu - \phi \tag{3.2}$$

where h is the Planck constant, ν is the frequency of the light and ϕ is the work function. The photovoltaic effect, on the other hand, is based on the generation and collection of the charge carriers and includes three simple processes. The first process is absorption, which creates charge carriers. The second is the separation of charge carriers by forming the p-n junction. The final step is to collect charge carriers at the terminals to produce the electricity.

In the absorption process, an incident photon with an energy equal to or higher than the material's bandgap energy is absorbed by the material. The absorbed photons excite the electron from the valence band to the conduction band. Excited electrons leave holes behind in the valence band. Both electrons and holes are charge carriers and both contribute to current. The process is illustrated in Figure 3.3. Since current depends on the amount of generated charge carriers, techniques that increase photon absorption, such as anti-reflection coating (ARC) or back mirror, are used.

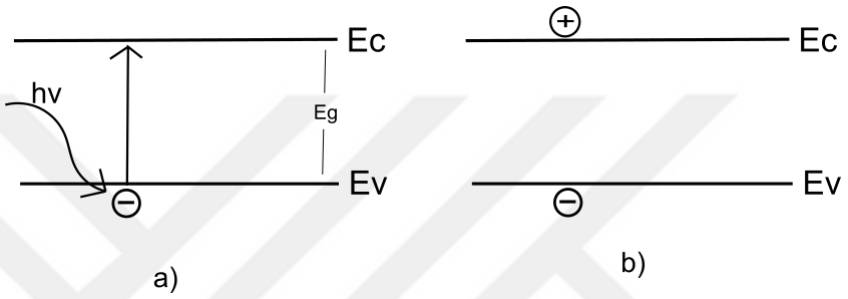

Figure 3.3. *(a) a photon with hv>Eg is absorbed by an electron (b) electron excited to the conduction with a hole in the valence band*

In milliseconds, the created electrons will return to the valence band and recombine with the holes. The recombination must be inhibited before happened to produce the electricity. The p-n junction is utilized to prevent recombination and separate charge carriers from one another. The p-n junction's built-in electric field separates the charge carriers before they recombine, as shown in Figure 3.4.

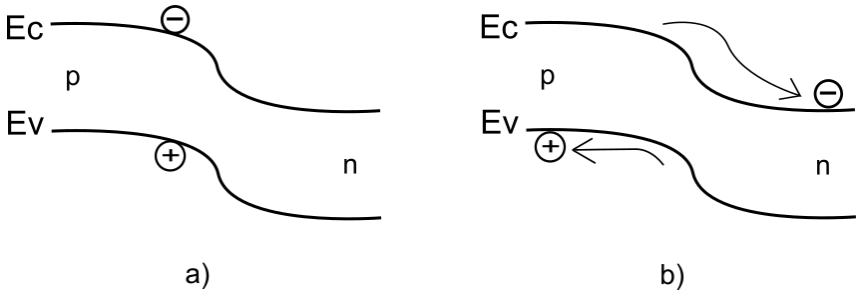

Figure 3.4. *(a) generated electron-hole pair (b) separation of carriers by the electric field*

Following separation, electrons are collected by the contacts on the n side, while holes are collected by the contacts on the p side. By connecting the device to a load in series, this photo-generated current is used to perform work.

The photovoltaic effect can also be used with p-i-n junctions, and solar cells with p-i-n junctions have been used in this thesis. The intrinsic layer (i) is placed between the p and n layers in the p-i-n junction. The same electric field is created with the same level of doping as in the p-n junction, but the depletion region is the largest fraction of the solar cell thickness in the p-i-n junction, therefore the electric field spreads across a larger region. In this configuration, the wider electric field improves the collection of charge carriers. Thus, the main mechanism in p-i-n solar cells is the drift of the charge carriers. In some applications, such as thin-film solar cells or in some cases when charge carrier separation is insufficient due to short lifetimes and short minority carrier diffusion lengths, p-i-n junctions can be preferred. However, using p-i-n junction may lead to some problems. The undoped i- region introduces series resistance to the solar cell and may result in lower conductivity. Nevertheless, p-i-n junction solar cells can be advantageous to use in solar cells that have a defective structure in terms of crystal quality. The band diagram of the p-i-n junction and its wider depletion region is illustrated in Figure 3.5.

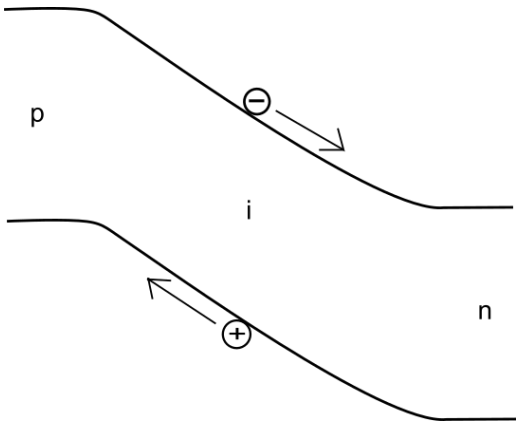

Figure 3.5. *Band diagram of a p-i-n junction*

Figure 3.6 shows a simple model of a p-n junction solar cell. The n-region of the solar cell is heavily doped and thinner, while the p-region is lightly doped and thicker. The net charge difference within the depletion region creates the electric field E_0. In

Figure 3.6, three steps of the photovoltaic effect can be seen. First, photons are absorbed within the solar cell. The point where a photon is absorbed varies with its energy and therefore wavelength. The depletion area and p-region at the back of the solar cell absorb the majority of photons. After the photon absorption, electron-hole pairs are generated. They are separated easily by electric field E_0 if they are absorbed within the depletion region. If not, they first diffuse into the depletion region and then drift via the electric field to the corresponding region. Finally, charge carriers are collected by the electrodes.

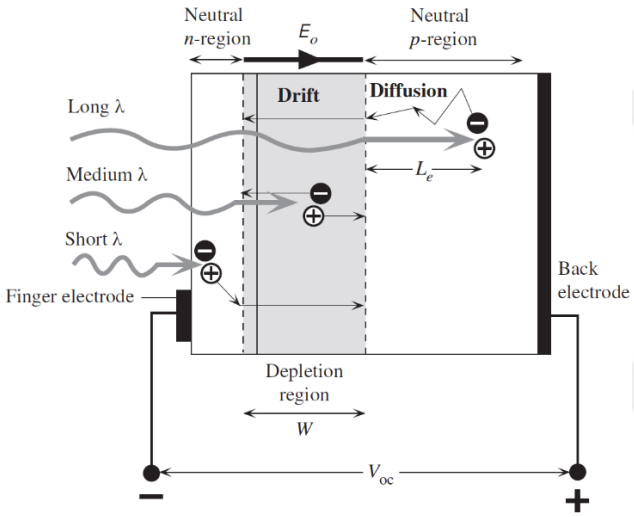

Figure 3.6. *A simple model of a solar cell [30]*

3.2. Basic Solar Cell Parameters

Solar cells behave like a diode under dark conditions and are given by the Shockley Diode Equation:

$$I = I_0[exp(\frac{qV}{kT}) - 1] \tag{3.3}$$

where I is the net current, I_0 is the dark saturation current, V is voltage applied between the contacts, q is electron charge, k is the Boltzmann constant and T is temperature in Kelvin. Under the illuminated conditions, (3.3) takes the form of:

$$I = I_0[exp(\frac{qV}{kT}) - 1] - I_L \tag{3.4}$$

where I_L is the current generated by the illumination. I-V curve of the solar cells under illumination is conventionally used as in Figure 3.7. Other key characteristics for solar cells can be derived from this curve.

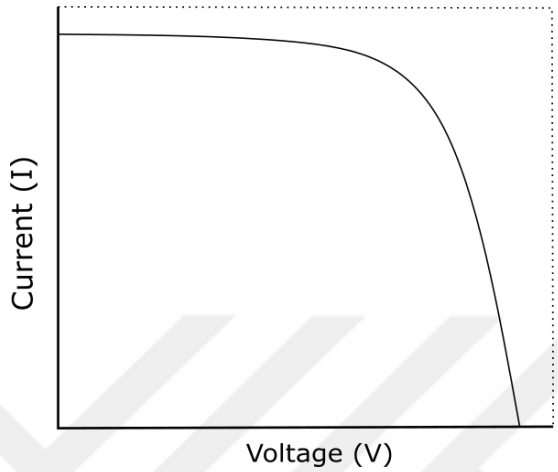

Figure 3.7. *Ideal I-V curve of a solar cell under the light*

For convenience, current density (J) versus voltage curve (J-V) is typically used instead of the I-V curve to cancel the effect of the cell area, where J can be found by the ratio of current to the cell area.

3.3.1. Short-Circuit Current (I_{sc})

Short-circuit current is the current that flows through a solar cell when there is no voltage applied between the cell's electrodes. Under the zero voltage conditions, $I_{SC} = I_L$ can be found from (3.4). I_{SC} is the maximum current that a solar cell can produce. Short-circuit current is affected by several factors, including cell area, light intensity, material's optical characteristics, and charge carrier collection probability.

3.3.2. Open-Circuit Voltage (V_{oc})

Open-circuit voltage is the voltage when no current passes through the solar cell. V_{oc} is the maximum voltage that a solar cell can produce. From (3.4), V_{oc} can be calculated as

$$V_{oc} = \frac{kT}{q} ln[\frac{I_L}{I_0} + 1] \quad (3.5)$$

Because this equation varies with the saturation current I_0, the value of the open-circuit voltage is mainly affected by the quality of the solar cell material.

3.3.3. Fill Factor (FF)

The fill factor is the parameter that determines the maximum efficiency a solar cell can produce. It is the ratio between the maximum power (P_{max}) generated by a solar cell and the product of I_{sc} and V_{oc}, as given in (3.6).

$$FF = \frac{I_{max}V_{max}}{I_{sc}V_{oc}} \quad (3.6)$$

In an ideal solar cell, FF is equal to 1, but in practice, it is always less than 1 due to the losses. The comparison of an ideal solar cell I-V curve and a real solar cell I-V curve has been given in Figure 3.8.

A fill factor less than 1 gives the curved I-V of a real solar cell rather than the perfect rectangular shape of an ideal solar cell where the fill factor is 1. For this reason, the fill factor is also known as the squareness of a solar cell's I-V characteristic.

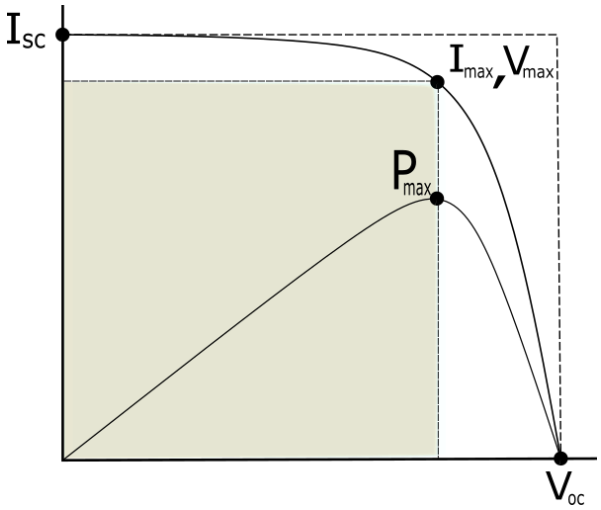

Figure 3.8. *Real and ideal solar cell I-V characteristic*

3.3.4. Conversion Efficiency (η)

The conversion efficiency is defined as the ratio of the power generated by the solar cell to the power density of the incident light. The conversion efficiency of a solar cell can be calculated using the following equation:

$$\eta = \frac{I_{sc}V_{oc}FF}{P_{in}} \tag{3.7}$$

where P_{in} is the power density of the incident light and is taken as the AM1.5 spectrum under the standard condition. The AM1.5 spectrum is The Standard Test Condition, with a power density of 1000W/m^2 at room temperature.

3.3.5. Parasitic Resistances

The generated power in solar cells is dissipated by the resistance effects of the solar cells. Shunt and series resistances are the two most common forms of parasitic resistance. The main influence of resistance effects is on the fill factor. Both types of resistance are illustrated in Figure 3.9 below.

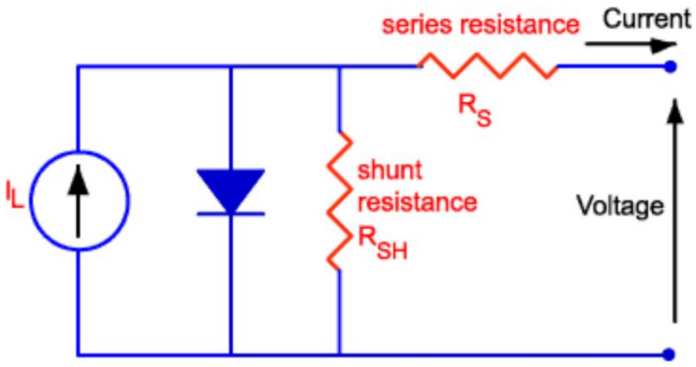

Figure 3.9. *Parasitic resistances [31]*

3.3.5.1. Series Resistance (R_s)

This type of resistance is caused by three factors: resistance in the bulk semiconductor, resistance at the interface between the semiconductor and the metal contacts, and resistance in the metal contacts. They all add up to give the solar cell's total

resistance. In an ideal solar cell, the series resistance is zero. The effect on a solar cell's I-V curve is illustrated below in Figure 3.10.

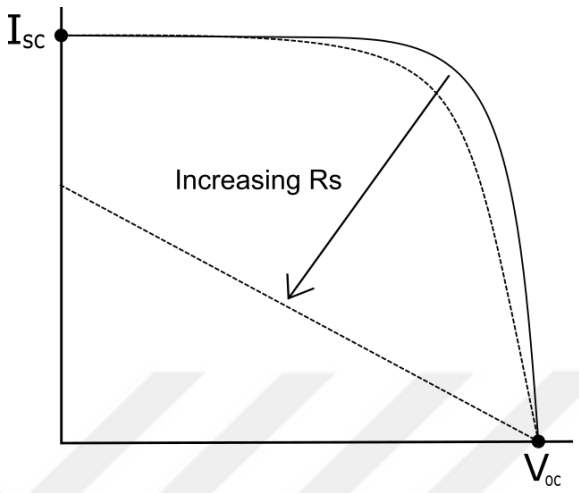

Figure 3.10. *The effect of the series resistance on the I-V curve*

3.3.5.2. Shunt Resistance (R_{sh})

Manufacturing defects cause shunt resistances. Instead of flowing through the semiconductor, light-generated current finds alternative paths to flow. To minimize such losses, shunt resistance must be as high as possible. Figure 3.11 shows the influence of the shunt resistance on the I-V characteristics.

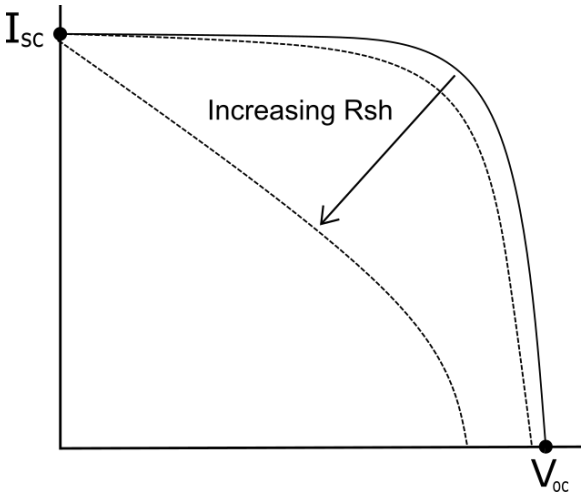

Figure 3.11. *The effect of the shunt resistance on the I-V curve*

3.3.6. Quantum Efficiency

The external quantum efficiency (EQE) is the fraction of charge carriers collected by metal contacts with incident light. It measures how well a solar cell converts incident light into electricity. The ideal shape of EQE is rectangular, however, due to recombination losses, the actual shape is lower and curved. Surface recombinations at the high-energy-short-wavelength region occur, and so do bulk recombinations at low-energy-long-wavelength, as seen below in Figure 3.12.

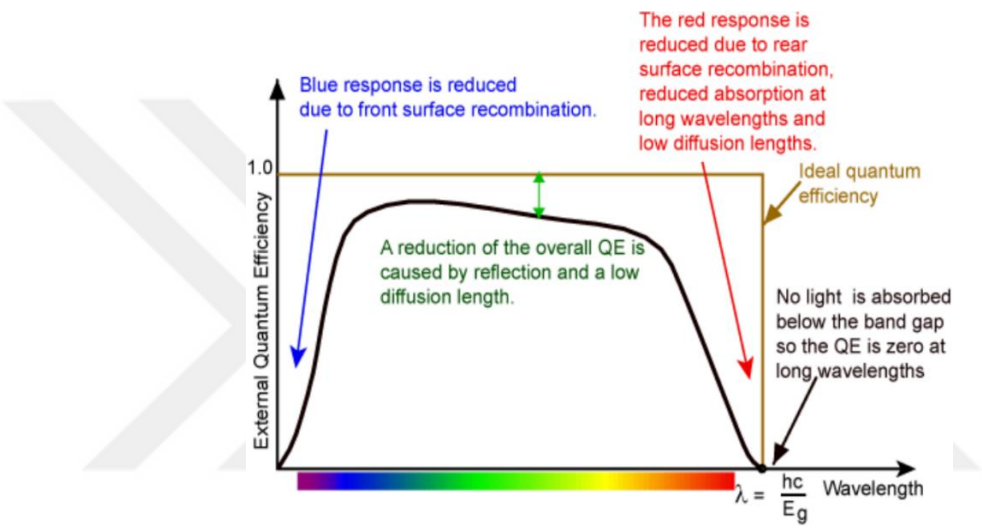

Figure 3.12. *The external quantum efficiency of a solar cell and corresponding losses to the light energy. [31]*

On the other hand, a solar cell does not absorb all incident photons due to reflection and transmission losses. This issue can be addressed by defining internal quantum efficiency (IQE). The internal quantum efficiency is the ratio of collected charge carriers to photons absorbed by solar cells. The internal quantum efficiency curve can be corrected from the external quantum efficiency curve by measuring the amount of loss that occurs due to reflection and transmission.

4. EXPERIMENTAL METHODS

4.1. Equipment

4.1.1 Molecular Beam Epitaxy (MBE)

Molecular Beam Epitaxy (MBE) is an advanced technique for producing high-quality crystalline materials. The process is carried out under ultra-high vacuum (UHV) conditions, with an ambient pressure on the order of ~10^{-10} Torr. Ultra-pure elements are heated until they slowly evaporate or sublimate in the individual effusion cells. The atom fluxes are directed towards a substrate, which is positioned and heated in the main chamber. The shutters which have an operating time of ~0.1 s control the atom flux. The low growth rates and the high rate of control enable precise control of abrupt interfaces and layer-by-layer material growth. Another advantage of the MBE method is the ability to monitor the process during the growth process. Reflection High-Energy Electron Diffraction (RHEED) is used to assess the cleanliness of the substrate surface prior to growth, calibrate the growth rate, get real-time growth rate feedback, and analyze surface morphology. In this thesis, solar cells have been produced by the Veeco GEN20MC MBE system (Image 4.1).

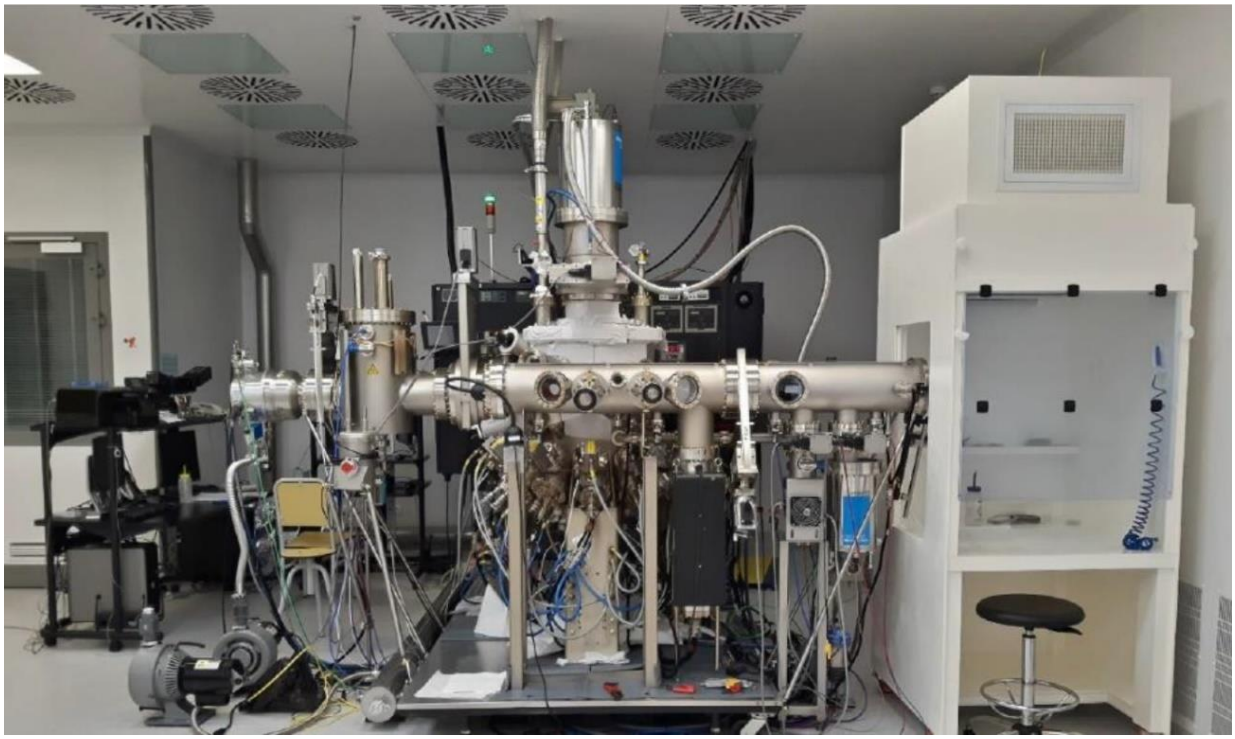

Image 4.1. *Veeco GEN20MC, Nanoboyut Research Laboratory*

4.1.2. High-Resolution X-Ray Diffraction (HRXRD)

The HRXRD is a characterization method that is used to determine the crystal's composition and quality, lattice strain-stress, layer thicknesses, mismatches, and dislocation densities [32]. The X-ray diffraction technique is based on wave interferences. In this process, electrons are accelerated by a high applied voltage and collide with a metal target. The rapid deceleration of electrons by the target results in x-ray radiation with the wavelength on the order of 0,1 nm. The generated X-rays are then directed at the sample. Incident X-ray beams will be diffracted by the sample's crystal planes, as illustrated in Figure 4.1.

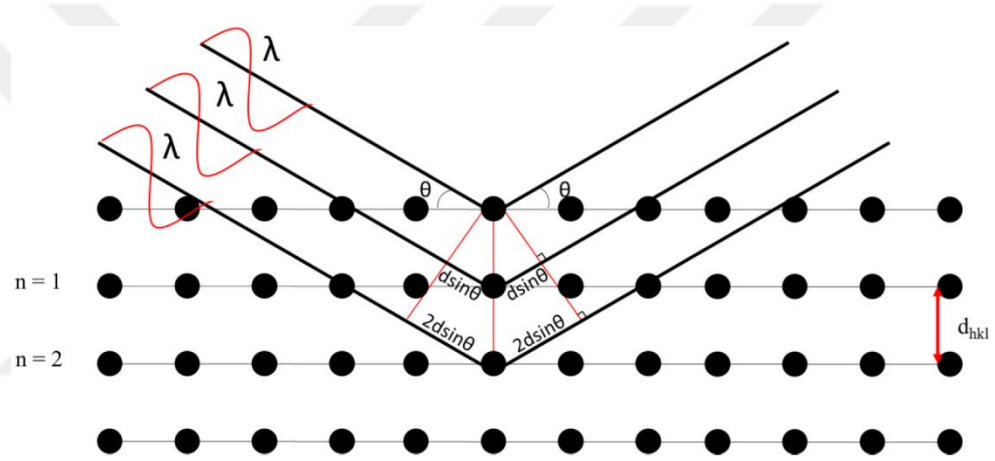

Figure 4.1. *Bragg diffraction by the crystal planes*

Diffraction occurs when the reflected beams interfere constructively with one other. The condition is given by Bragg's law:

$$n\lambda = 2d_{hkl}\, sin\, \theta \qquad (4.1)$$

where n is a positive integer, λ is the wavelength of the incident X-ray beam, d_{hkl} is the lattice plane spacing and θ is the angle of incidence.

4.1.2.1. Rocking Curve (RC)

The RC measurement is used to analyze crystal defects such as dislocation density, curvature, misorientation, and inhomogeneity. In the diffraction graph, a perfect crystal generates a sharp and narrow sudden peak. Information about the crystal quality is obtained by using the full-width-at-half-maximum (FWHM).

The Panalytical X'Pert Pro MRD system has been used to conduct HRXRD measurements in this thesis to investigate the structural characteristics of GaAs/Si solar cells (Image 4.2.).

Image 4.2. *Panalytical X'Pert Pro MRD, Nanoboyut Research Laboratory*

4.1.3. Scanning Electron Microscope (SEM)

SEM is an imaging technique that produces magnified surface images of the materials by using an electron beam instead of visible light. The fundamental principle of the SEM is based on wave-particle duality. Because electrons have a much smaller wavelength than visible photons, significant magnification of the image is produced. The SEM is made up of an electron gun, electromagnetic lenses, and a detector. The electron beam is accelerated and then focused onto a sample by electromagnetic lenses. Electrons interact with the atoms in the sample and produce a variety of signals as shown in Figure

4.2. In the SEM, high-resolution images are created by detecting secondary electrons and backscattered electrons. The number of detected electrons depends on the variations of the sample surface which results in the image of the topography of the sample surface.

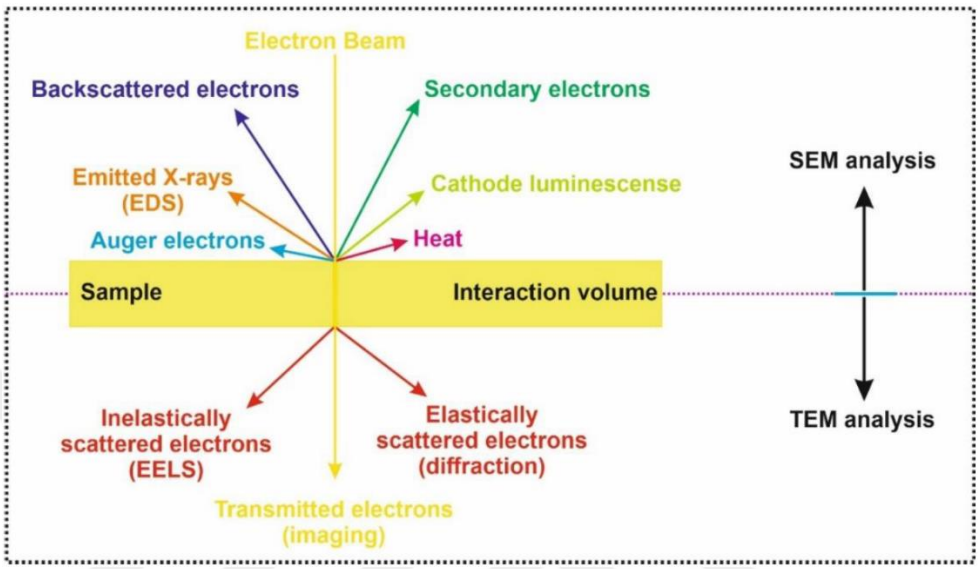

Figure 4.2. *Produced signals by electron-matter interaction [33]*

The SEM is used in this study to examine the surface morphology of GaAs layers on Si substrates.

4.1.5. Photoluminescence Spectroscopy (PL)

PL is a useful technique for investigating the optical and electrical properties of semiconductors and molecules. It is simple and quick to use because no sample preparation is required and measurements can be performed without making contact. It provides information about the structure's impurities and defects. The fundamental principle behind the PL is photoexcitation and radiative recombination of charge carriers. Incident light with an energy greater than the semiconductor's bandgap energy is absorbed by the sample. Absorbed photons generate electrons in the conduction band and holes in the valence band. Depending on the material characteristics, the excited electrons will return to their equilibrium state in the valence band after some time. This radiative recombination process can be in different forms, as shown in Figure 4.3. Eventually,

electrons and holes recombined and emit photons with an energy that is dependent on the recombination process. Ideal semiconductor gives narrow and sharp peaks in the measurement results. When impurities are introduced, the sharpness is decreased.

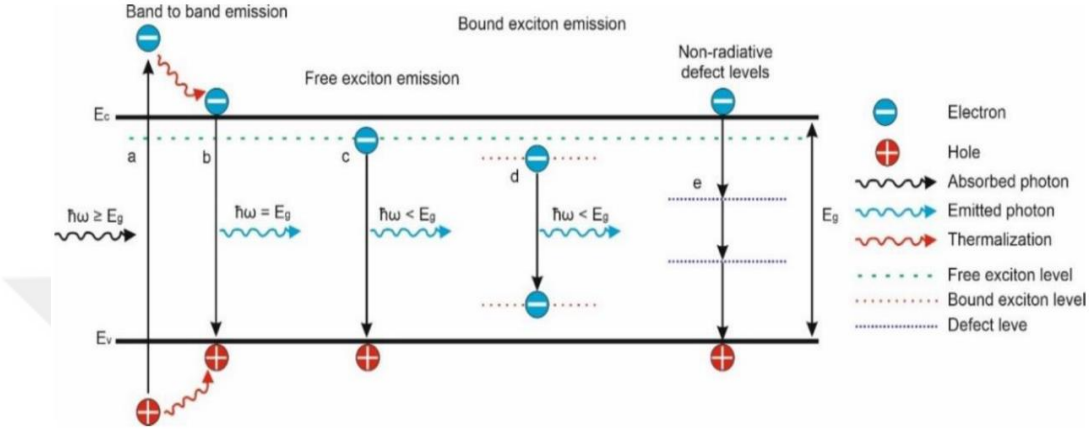

Figure 4.3. *Various recombination processes in a semiconductor [34]*

BrukerVERTEX80/80v model Fourier Transform Infrared (FT-IR) spectrometer has been used in this work to make PL measurements and inspect the characteristics of the solar cells (Image 4.3).

Image 4.3. *Bruker VERTEX80/80v FT-IR Spectrometer, Nanoboyut Research Laboratory*

4.1.6. Physical Vapor Deposition (PVD)

Physical vapor deposition (PVD) is a general name for thin-film coating methods. The PVD principle is based on the vaporization of the solid source and its condensation on the substrate surface. To minimize contaminations, the process must be carried out in a high vacuum environment, on the order of 10^{-6} Torr. The thickness of the coating on the substrate can be monitored by a thickness monitor. There are several methods to coat thin films using the PVD, in this thesis thermal evaporation, electron beam evaporation and sputtering are used. The equipment used for coating thin films is the VAKSIS-Midas PVD system which contains magnetron sputtering, thermal evaporation, and electron beam evaporation (Image 4.4).

4.1.6.1. Thermal Evaporation

Thermal evaporation is one of the widely used metal thin film deposition techniques. In this type of evaporation, the source material is placed onto the resistive boat and a high electric current is applied through a resistive boat to heat it. The resistive boat is started to heat the source. When the solid source is melted, the shutter is opened and deposition begins. The vaporized metal atoms are recondensed on the surface of the substrate and form the thin layer coating.

4.1.6.2. Electron Beam Evaporation

Electron beam evaporation is another evaporation technique that is used to evaporate the source material and deposit it on the substrate. Instead of resistive heating by tungsten, an electron beam is used as a vaporizer in electron beam evaporation. The electron beam is accelerated to high kinetic energy and directed toward the source to be vaporized. The kinetic energy of the electrons is transformed into thermal energy, which heats and evaporates the source. Evaporated atoms condense on the surface of the substrate resulting in the formation of a thin film.

4.1.6.3. Magnetron Sputtering

Sputtering is widely used in the deposition of metals, insulators and alloys. The sputtering system uses ion bombardment to deposit thin films. Argon is commonly used as a plasma source in sputtering systems to bombard the target material. Using DC plasma power and sustained Argon flow, the energetic Argon ions hit the target surface, physically ejecting atoms and redepositing them on the substrate surface.

Image 4.4. *VAKSIS-Midas PVD system, Nanoboyut Research Laboratory*

4.1.7. Quantum Efficiency Measurement

The measurement of quantum efficiency is used to provide information about the junction quality, recombination dynamics and response of a solar cell to the incident photon's wavelength. As mentioned in Chapter 3, in this measurement light-generated charge carriers are collected by probes. The ratio of collected light-generated charge carriers to incident photons is measured and visualized as a function of wavelength. Newport Quantax300 system is used in this work to obtain external and internal quantum measurements of the solar cells (Image 4.5).

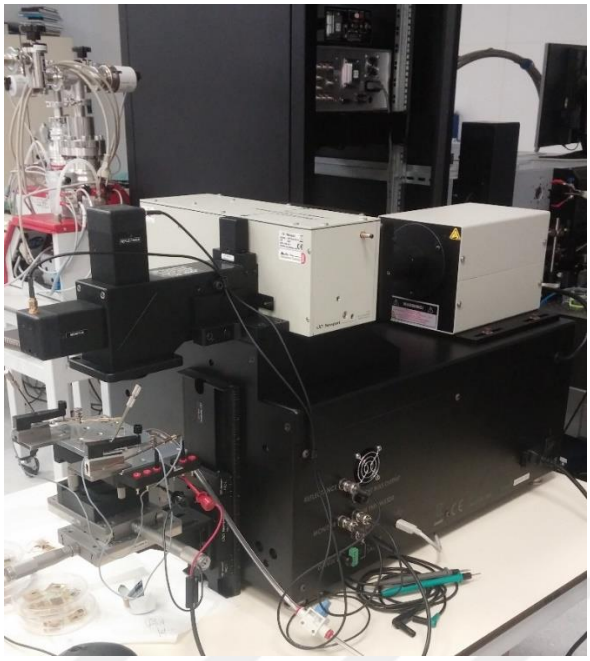

Image 4.5. *Newport Quantax300 system, Nanoboyut Research Laboratory*

4.1.8. I-V Measurements

I-V measurements are done at the end of the solar cell fabrication processes to examine the performance of the solar cells. Under illumination, the current characteristic of a solar cell is measured relative to the voltage by probes. Measurement results can be used to compute the PCE, short-circuit current, open-circuit voltage, fill factor, series resistance, and shunt resistance. In this thesis, an AM1.5G calibrated ABET 2000 solar simulator is used (Image 4.6).

Image 4.6. *ABET 2000 AM1.5G Solar Simulator, Nanoboyut Research Laboratory*

4.2. Fabrication Procedure

In Nanoboyut Research Laboratory, the first study on ELO GaAs/GaAs solar cells is studied by Zaimler [35]. The growth of III-V semiconductors on Si substrates is studied by Arpapay et al. [26, 36, 37] and Aktaş [27]. In Aktaş's study, dislocation filters and growth parameters for heteroepitaxial growth of GaAs on Si were widely investigated. Using the experience and knowledge gained from previous studies, Büyükpınar [38] has studied p-n type GaAs thin-film solar cells peeled-off from Si substrates using the Heteroepitaxial Lift-Off (HELO) method. In his study, an efficiency of 4.52% was achieved for the first time. In this study, previous results are tried to be improved using the p-i-n type junctions.

The fabrication process of the solar cells is explained in this subheading. The overall fabrication process flow is shown in Figure 4.4.

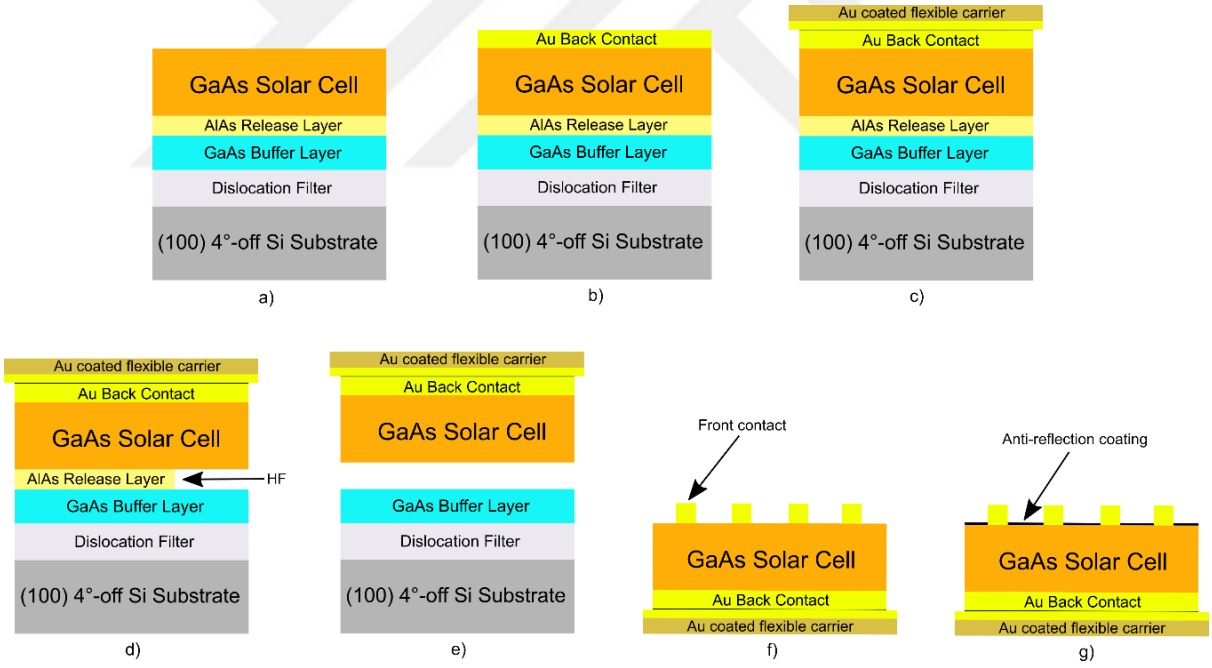

Figure 4.4. *a) Newly grown GaAs/Si, b) Au back contact metallization, c) Au-Au bonding by thermocompression, d) dissolution of AlAs release layer, e) completed separation of substrate and thin film, f) front contact metallization, g) anti-reflection coating*

4.2.1. Design Consideration

In this thesis, GaAs solar cells were produced on Si substrates using the Veeco GEN20MC solid-source MBE system in the Nanoboyut Research Laboratory. The substrate for GaAs solar cells is 3" phosphorus (P) doped Czochralski (CZ) Si wafers with a resistivity of 1-10 Ω.cm, a thickness of 381 µm, and orientation of (100) with 4° offcut. Dislocation filter approaches such as strained-layer superlattice (SLS), step-by-step AlGaAs/GaAs growth in thermal cycle annealing (TCA), and quantum dots (QDs) are employed to minimize dislocations in GaAs/Si solar cells in this study while it is not necessary for GaAs/GaAs reference solar cells. To improve on the previous results from Büyükpınar's study, solar cells were grown in the form of a p-i-n junction with n- emitter and p- base. The n- layer is doped with Si and the p- layer is doped with beryllium (Be). For convenience, thin-film GaAs solar cells separated from Si substrates will be referred to as HELO GaAs solar cells while thin-film GaAs solar cells separated from GaAs solar cells will be referred to as ELO GaAs solar cells. The schematics of GaAs/Si and GaAs/GaAs solar cells are illustrated in Figure 4.5.

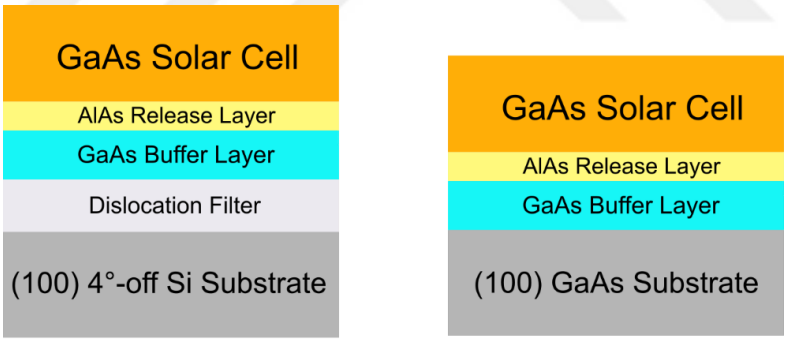

Figure 4.5. *Cross-section of a) GaAs/Si and b) GaAs/GaAs solar cells*

4.2.2. Back Contact Metallization

The backside of the solar cells must be coated with metal to extract photo-generated current to an external load. Gold (Au) was deposited to the rear side of the solar cells in this study not only for current extraction but also for bonding with a gold-coated flexible carrier. Back contact metallization requires a clean epitaxial layer surface. As a result, to avoid contamination, solar cells must be loaded into the vacuum chamber for electron

beam evaporation immediately following MBE growth. After loading, a 200 nm Au layer was deposited by electron beam evaporation to create an ohmic contact. Figure 4.6 shows the structure following back contact metallization. Following metallization, the wafer was cleaved into smaller samples of about 1-1.5 cm^2 to be ready for bonding with flexible carriers.

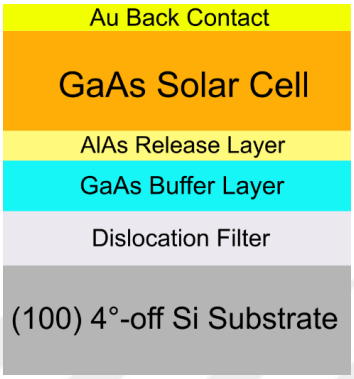

Figure 4.6. *Schematic of solar cells after the back contact metallization*

4.2.3. Epitaxial Lift-off Process

Three steps are included in ELO processes in this study. First is the deposition of gold to flexible carriers. Second, bonding gold-coated flexible carriers with the gold-coated solar cells by thermocompression bonding. Finally, dissolution of AlAs release layer in HF solution.

4.2.3.1. Gold Deposition of Flexible Carriers

In this work, 50 and 75 μm polyamides were used as flexible carriers. Because of poor adhesion of gold to polyamides, first 20 nm platinum (Pt) were deposited to polyamides by the sputtering system, then 200 nm Au deposited by the thermal evaporation system.

4.2.3.2. Thermocompression Bonding

Thermocompression bonding is a metal-metal bonding method under temperature and pressure. Cleaved samples and gold-coated flexible carriers were bonded together under a pressure of 0.3-0.5 MPa and a temperature of 160 ℃ for as long as 10 minutes.

The illustration of the bonding process is shown in Figure 4.7 (a) and (b), and a photograph of a bonded sample and flexible carrier is shown in Figure 4.7 (c).

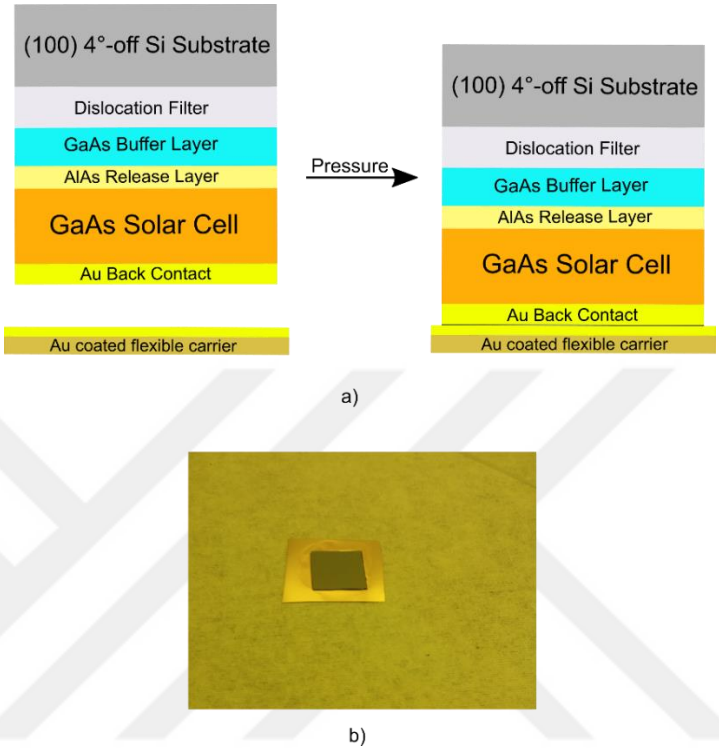

Figure 4.7. *(a) Before the thermocompression (b) after the thermocompression processes. (c) bonded GaAs/Si sample to gold-coated polyamide*

4.2.3.3. Dissolution of Release Layer

To obtain thin-film solar cells, the AlAs release layer must be etched after the bonding step. In this work, a 15 nm AlAs release layer was grown by MBE between the substrate and solar cell layer. The AlAs layer was selectively etched away using an aqueous 38-40% HF solution. The etching process was carried out in a plastic closed vessel since HF is extremely dangerous. The etch rate of solar cells and substrates has been measured around 8-9 mm/h at room temperature.

Following the dissolving of the AlAs layer, both the ELO cell and the substrate must be cleaned to remove chemical contaminants. For 3 minutes each, the samples were washed with acetone, isopropyl alcohol, and an HCl: H_2O (1:10) solution. Finally, samples were washed with deionised (DI) water then dried with filtered nitrogen (N_2) and ready for the next process. Substrates, on the other hand, require CMP before they

can be used in the next growth step. The dissolution process is shown in Figure 4.8 (a) and (b), and an example of a separated thin-film solar cell and a substrate in Figure 4.8 (c).

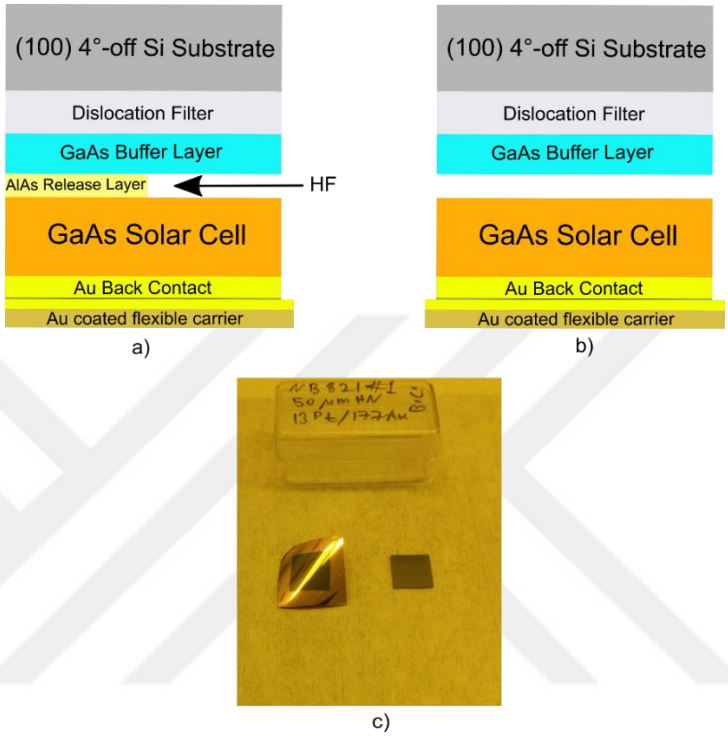

Figure 4.8. *a) Dissolution of AlAs release layer, b) after the dissolution of AlAs layer, c) separated a thin-film solar cell and a substrate*

4.2.4. Front Metallization

The next step is to put metal terminals on top of the device to collect photo-generated carriers. In contrast to backside metallization, the top contacts of a cell have a grid design to prevent the top contacts from blocking incident light.

Top contact metallization was completed employing both poly-Si shadow masks and lithography. Thermal tapes were used to adhere shadow masks to the surfaces of solar cells. An open space at the edge of the cells was left, otherwise, a short-circuit would take place in the solar cell after the top contact metallization. The front surface of the solar cells was deposited with Ni/Ge/Au as 35/70/500 nm using the electron beam evaporation system. Following top contact deposition, the sample was annealed for 15 minutes on a hot plate at 300 ℃ to create Ohmic contacts. Finally, the cap layer was etched until it

reached the window layer. The etching process was carried out with a 25:5:200 dilution of citric acid ($C_6H_8O_7$): hydrogen peroxide (H_2O_2): water (H_2O) solution. Figure 4.9 (a) and (b) illustrate a model of cell structure and a photograph of a solar cell after top contact metallization.

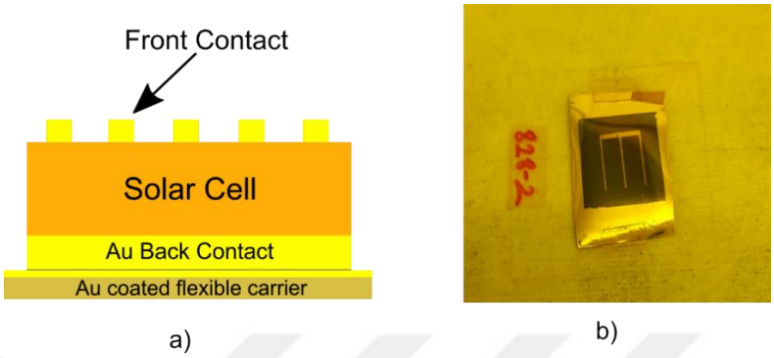

Figure 4.9. *(a) after the front contact metallization and (b) a photograph of thin-film solar cell*

4.2.5. Anti-Reflective Coating

Reflection is one of the main loss mechanisms in solar cells. The reflection of incident light from the bare GaAs surface corresponds to 30-35% loss [39]. An anti-reflective coating (ARC) must be applied to the front surface to minimize reflection. After coating with ARC, the loss value in the 400-850 nm region can be reduced to 3%, resulting in better external quantum efficiency of the solar cells. In this thesis, a thickness of 48 nm ZnS and a thickness of 100 nm MgF_2 were deposited onto solar cell surfaces using the sputtering system and electron beam evaporation, respectively. Figure 4.10 (a) and (b) show the representation of cell structure and a photograph of a solar cell after ARC deposition.

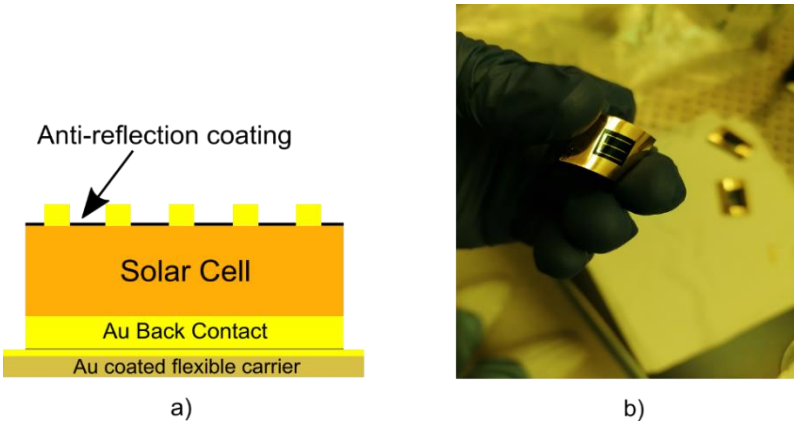

Figure 4.10. *(a) after the ARC coating and (b) a photograph of thin-film solar cell*

5. EXPERIMENTAL RESULTS

5.1. Scanning Electron Microscope

Samples were grown using QDs, SLSs, Si substrates with 4° offcut and AlGaAs/GaAs layer-by-layer growth with TCA as dislocation filters to examine the dislocations due to heteroepitaxial growth. SEM images of the samples were taken to analyze the surface morphology.

QDs have the ability to bend dislocation lines and prevent them from reaching the surface of the sample. To employ this, samples were first grown with 10-period InAs QDs on Si (100) substrates. Image 5.1 (a) shows that the QDs approach alone is insufficient to prevent anti-phase domains (APDs). For the following sample (Image 5.1 (b)), QDs were used with 4° offcut (100) Si substrates as dislocation filters. SEM images reveal that APDs are prevented with these dislocation filters. However, the crystal's quality was not as desired, and stepped structures formed on the surface of the sample.

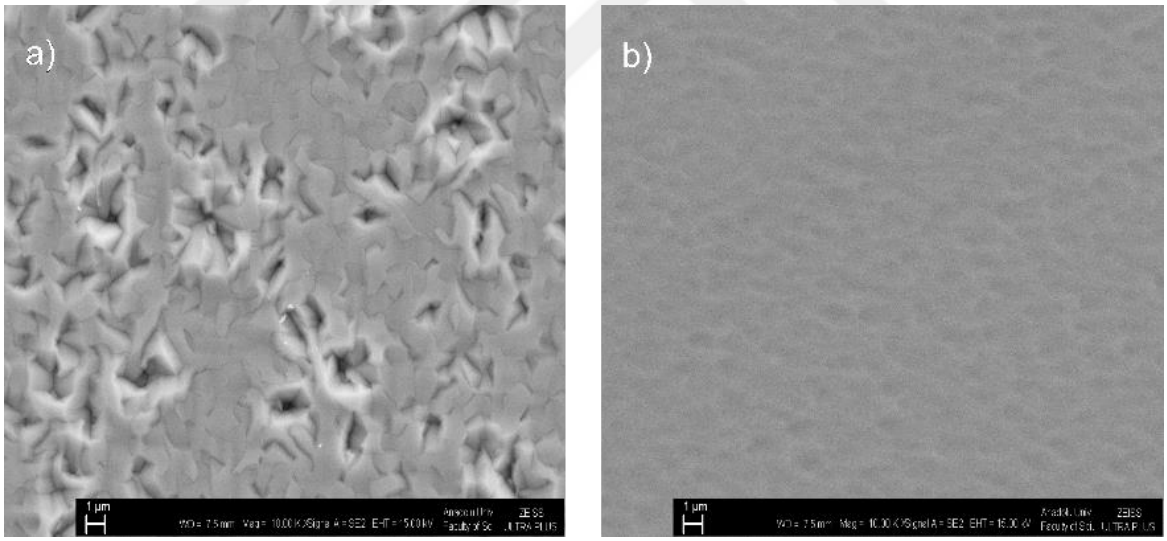

Image 5.1. *SEM images of (a) GaAs/Si with QD (b) GaAs/Si with QD and 4° offcut Si substrate*

Generated strain fields by the SLSs can bend dislocation lines, making them parallel to the surface and reducing the dislocations in the active device. The samples were grown with InGaAs SLSs to examine their impact on dislocation reduction. Following the prior results obtained with 4° offcut Si substrates, all the subsequent samples were grown with 4° offcut (100) Si substrates in addition to dislocation filter approaches. Also, both the

InAs QD and InGaAs SLS approaches were used on one sample to investigate the combined effect of QDs and SLSs on dislocations. Image 5.2 (a) and (b) show that APDs were prevented, stepped structures and surface roughnesses were also reduced compared to previous results. As a result, SLS dislocation filters with 4° offcut Si substrates were concluded to be superior to QD dislocation filters with 4° offcut Si substrates. However, combining QD and SLS approaches resulted in increased roughness and stepped structure on the surface of the sample.

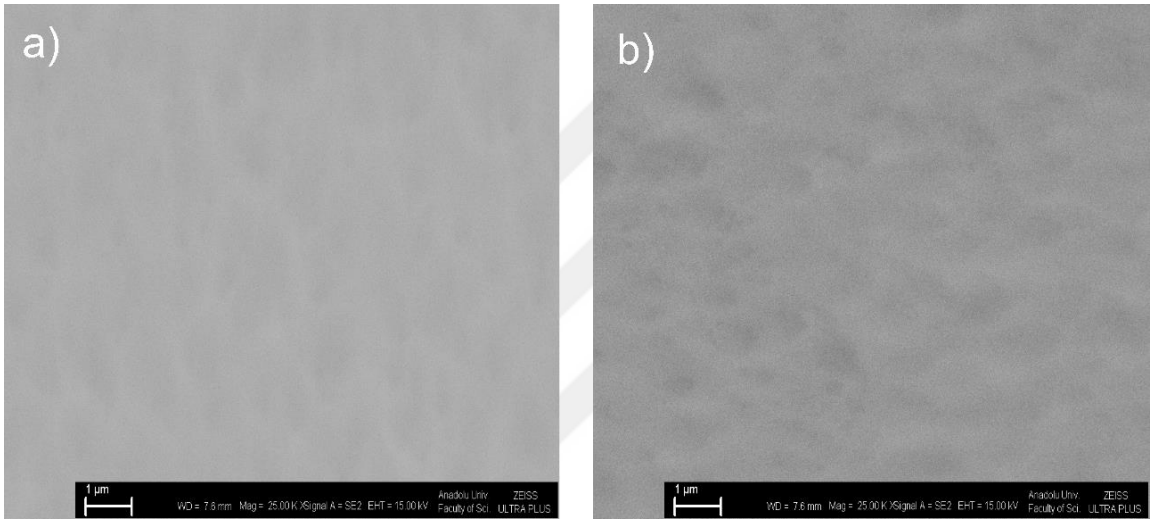

Image 5.2. *SEM images of (a) GaAs/Si with SLS (b) GaAs/Si with QD and SLS*

TCA is another approach for reducing dislocations that do not require any strain in the crystal to bend the dislocations. Heat treatment during crystal growth has a direct influence on dislocations and enables dislocation migration. As the final method for reducing dislocations, the step-by-step AlGaAs/GaAs growth with TCA approach was used as a dislocation filter. Image 5.3 shows the surface morphology of a TCA-grown sample. Just as the SLS approach, APDs have successfully been annihilated, and roughness was reduced. In terms of SEM analysis, the best surface morphologies were obtained using SLS and step-by-step AlGaAs/GaAs with TCA. In the following section, XRD analyses were performed to compare the SLS and step-by-step growth with TCA approaches.

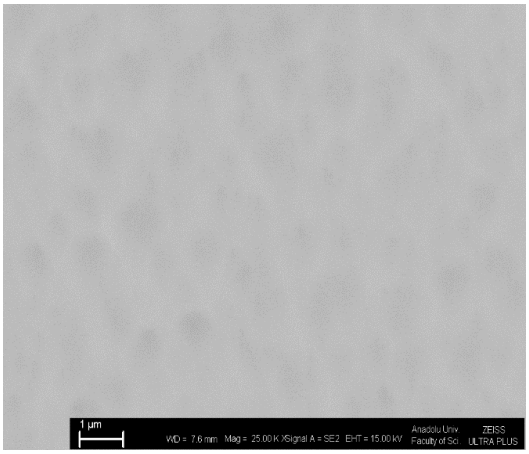

Image 5.3. *SEM image of GaAs/Si with step-by-step AlGaAs/GaAs growth with TCA*

5.2. High-Resolution X-ray Diffraction

The omega-2theta scan aligned at (004) GaAs reflection point plane of the GaAs/Si samples with SLS and GaAs/Si samples with step-by-step growth with TCA is shown in Figure 5.1. Separate peaks produced by the Si substrate, GaAs layer, and the InGaAs/GaAs SLS fringes can be seen in this figure. The peak position of the SLS-grown GaAs sample is 33.055º while the peak position of the step-by-step and TCA-grown GaAs sample is 33.0552º. The produced peak positions are very close to the theoretical value since the theoretical value of GaAs is centered at θ=33.0548º. This slight shift to larger degrees is expected as a result of the small amount of compressive stress in the growth plane.

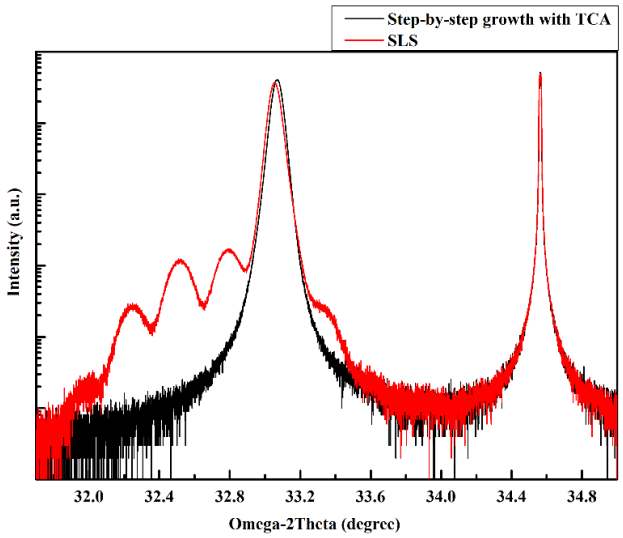

Figure 5.1. *Omega-2theta scan aligned at (004) reflection of GaAs/Si with step-by-step w/ TCA and GaAs/Si with SLS*

The FWHM value of the diffraction peak of SLS-grown GaAs layers is 203 arcsec, while step-by-step with TCA-grown GaAs has a value of 190 arcsec. In addition, the RC of both TCA-grown and SLS-grown samples are given in Figure 5.2. From the RC curve, the calculated FWHM value of the SLS-grown sample is 205 arcsec and is 191 arcsec for the step-by-step with TCA-grown sample. A high FWHM value indicates a vast amount of dislocations and strain in the crystal, resulting in a broadening of the diffraction peak and reduced intensity. Hence a lower FWHM value means better crystal quality. As a result, step-by-step AlGaAs/GaAs growth with TCA-grown GaAs layers has better crystal quality than SLS-grown GaAs layers.

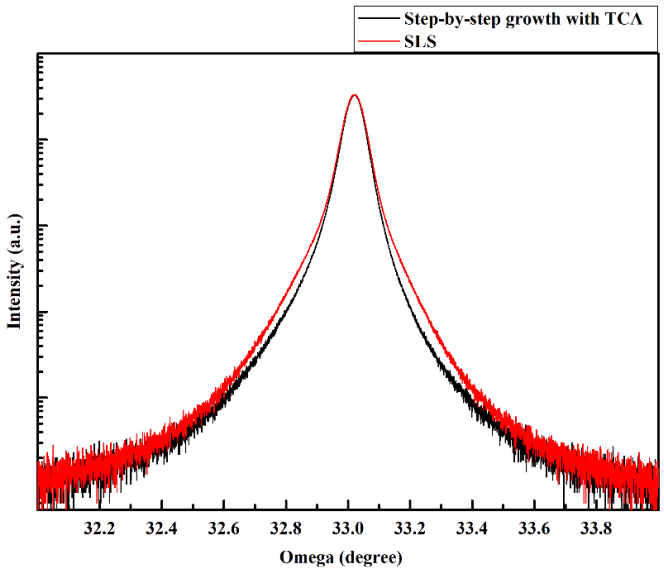

Figure 5.2. *The rocking curve of GaAs/Si with TCA and GaAs/Si with SLS*

Based on SEM and HRXRD results, step-by-step AlGaAs/GaAs growth with TCA-grown samples are understood to be the better approach for growing high-quality GaAs layers on Si. All the subsequent GaAs/Si solar cells were produced using this approach. After deciding the dislocation filter approach, some growth parameters were adjusted and optimized to improve crystal quality. Figure 5.3 shows the final RC and Omega-2Theta scans of the solar cells used in this thesis. The Omega-2Theta scan has an FWHM value of 159 arcsec and the RC has an FWHM value of 151 arcsec.

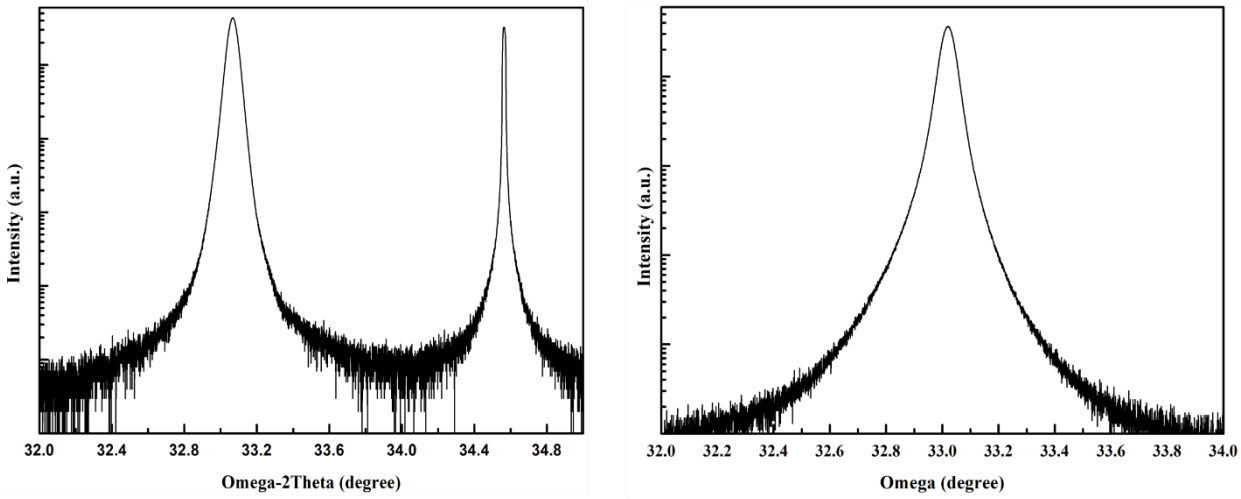

Figure 5.3. *Omega-2Theta scans and RC graphs of solar cells using step-by-step growth with TCA*

5.3. Photoluminescence Spectroscopy

In Figure 5.4, the PL spectrum at room temperature of three different regions of GaAs/Si samples is given (major, minor, and center) to demonstrate the homogeneity through the substrate. Because no shift toward longer or shorter wavelengths was observed, the sample is structurally homogeneous. On the other hand, the intensity of the PL spectra varies slightly from region to region. This could be the result of instantaneous measurement conditions. Overall, grown samples can be considered homogeneous.

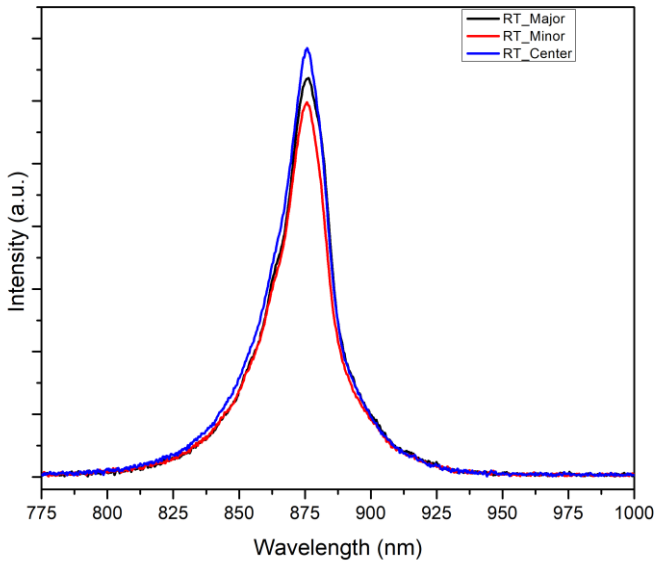

Figure 5.4. *PL spectra of GaAs/Si solar cells at room temperature*

Figure 5.5 shows the PL spectra of GaAs/GaAs solar cells and GaAs/Si solar cells before and after the lift-off process. GaAs/Si solar cells peaked at 875.8 nm (1.416 eV) and the reference GaAs/GaAs solar cells peaked at 870.7 nm (1.424 eV) (Figure 5.5 (a)). The intensity of emission peaks of GaAs/GaAs solar cells is higher more than 10 times than that of GaAs/Si solar cells as expected, which indicates non-radiative recombination traps in the heteroepitaxial GaAs. After the separation of the active device layer and transferring to the polyamide carriers, the emission peaks of the thin-film solar cells showed shifting towards lower energy and their emission intensity was observed to be decreased (Figure 5.5 (b)). It is also seen that the valance band (heavy hole - light hole) splits into two distinct peaks as A and B. Tensile strain induced by heteroepitaxial growth is responsible for the red shifting of the bandgap and the splitting of the valance band [40, 41].

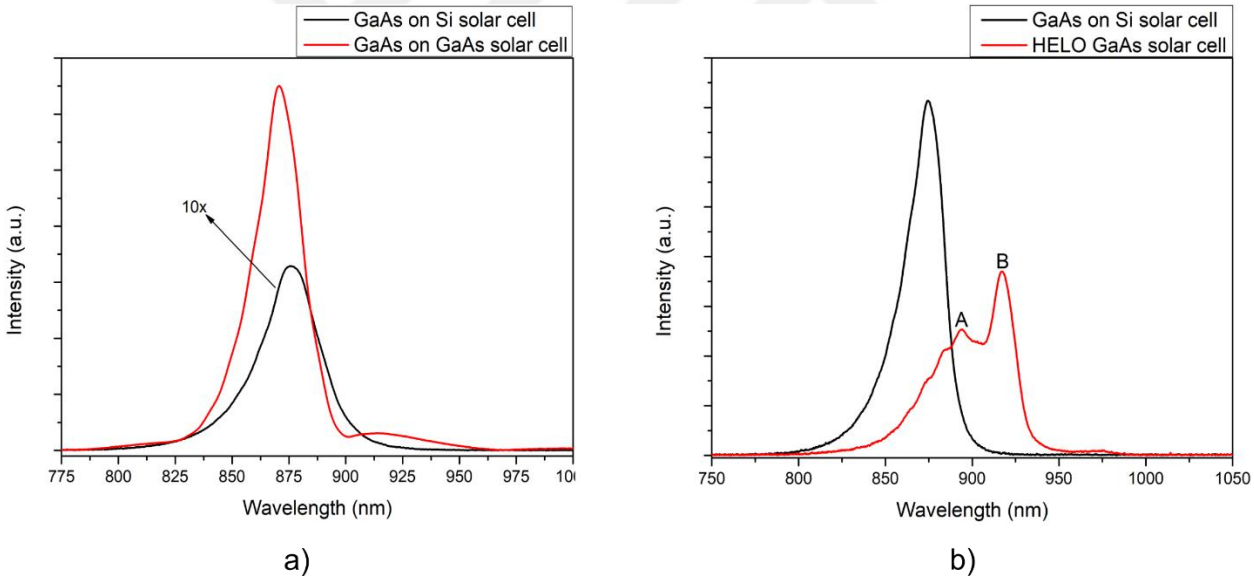

Figure 5.5. *PL spectra of (a) GaAs/Si vs GaAs/GaAs solar cells before the separation and (b) GaAs/Si vs separated HELO GaAs solar cells*

Figure 5.6 shows the PL spectrum of a HELO GaAs solar cell and the separated substrate of a solar cell with a buffer layer on top. The emission intensity of HELO solar cells is significantly higher than that of the buffer layer, indicating that HELO solar cells have higher crystal quality than the buffer layer. This is due to the AlAs release layer, which also works as a filter layer between the buffer layer and the active device layer.

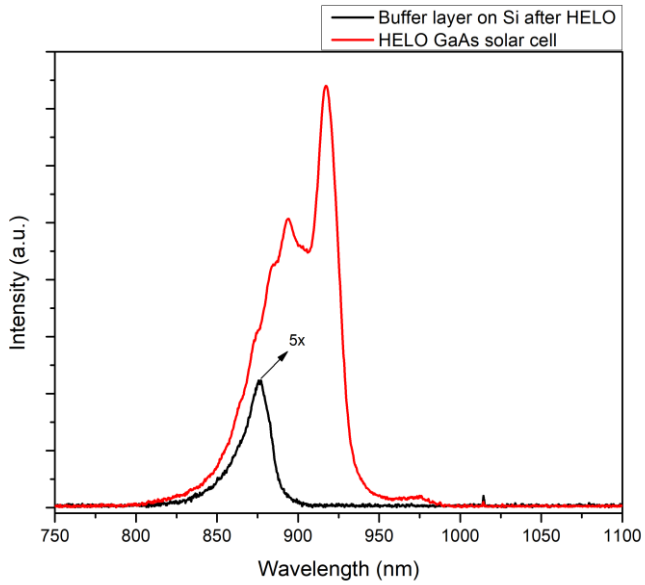

Figure 5.6. *PL spectra of HELO GaAs solar cell and its buffer GaAs layer on the separated Si substrate*

5.4. Quantum Efficiency

Following the fabrication processes, QE measurements were taken to assess the quality of the produced thin-film solar cells. In the scope of this thesis, heteroepitaxial p-i-n type thin-film solar cells were fabricated and compared to reference homoepitaxial p-i-n type thin-film solar cells. Furthermore, heteroepitaxial p-n type thin-film solar cells were fabricated and compared to p-i-n type thin-film solar cells to assess the difference between them. Also, from the EQE results of the solar cells, J_{sc} can be calculated over the spectrum. The formula to calculate J_{sc} is [42]:

$$J_{sc}(\lambda) = -q \int_{\lambda_1}^{\lambda_2} EQE(\lambda)\, \Phi_{ph,\lambda}^{AM1.5}\, d\lambda \tag{5.1}$$

where $\Phi_{ph,\lambda}^{AM1.5}$ is the spectral photon flux under the standard condition AM1.5.

First, 1.5 µm p-i-n type HELO solar cells as the subject of this thesis' results are given. In Figure 5.7, quantum efficiency results and reflection measured in the range of 350-950 nm are displayed. As can be seen, the quantum efficiency of the short wavelength region is lower than that of the longer wavelength region. This is because GaAs has a high absorption coefficient, which causes more absorption near the surface and surface recombination. To reduce short-wavelength losses, different window layer approaches

are required. The quantum efficiency response of the long-wavelength region in the range of 600-840 nm is approximately 80-90%. The good response of the long-wavelength region is due to the use of a p-i-n type solar cell, wider depletion region aided the charge extraction and toleranced the defects and dislocations due to the heteroepitaxial growth. Also, reflection throughout the measured spectrum was found to be around 1%. Because of the good ARC, internal and external quantum efficiencies are nearly equal and indicate no loss occurred due to reflection. Also, the integrated J_{sc} value of the HELO p-i-n solar cell is found to be 22.81 mA/cm^2.

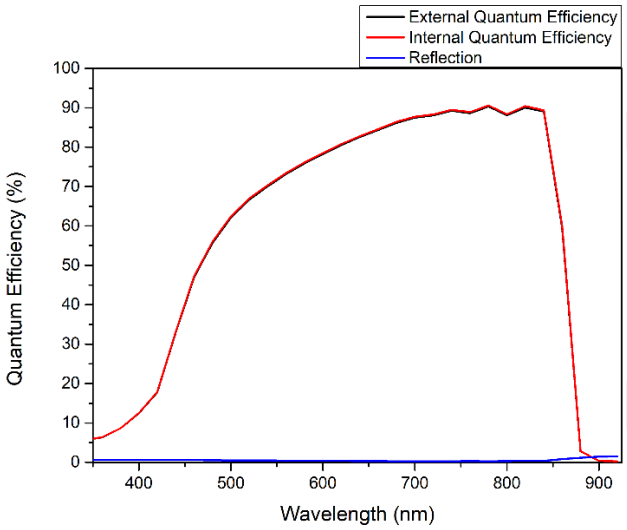

Figure 5.7. *Quantum efficiency and reflection results of HELO p-i-n solar cells*

Figure 5.8 depicts a comparison of HELO p-n type GaAs solar cells and HELO p-i-n type GaAs solar cells. The results of the EQE measurements show that the short-wavelength region response of both types of solar cells is approximately similar. However, a big response difference occurred in the long-wavelength region. In the p-n junction solar cell, minority carriers couldn't reach the depletion region before recombining. Due to this short diffusion length of minority carriers, large losses took place on the backside of solar cells. Since p-i-n type solar cells are used in this thesis, this comparison demonstrates the success of using p-i-n type solar cells to improve the solar cells' long-wavelength response over p-n type solar cells with short diffusion length of minority carriers. The wider depletion region in the p-i-n type solar cell aided the extraction of charge carriers and improved the long-wavelength region's response of the solar cell. Integrated J_{sc} value of HELO p-n type solar cell was found to be 19.6 mA/cm^2.

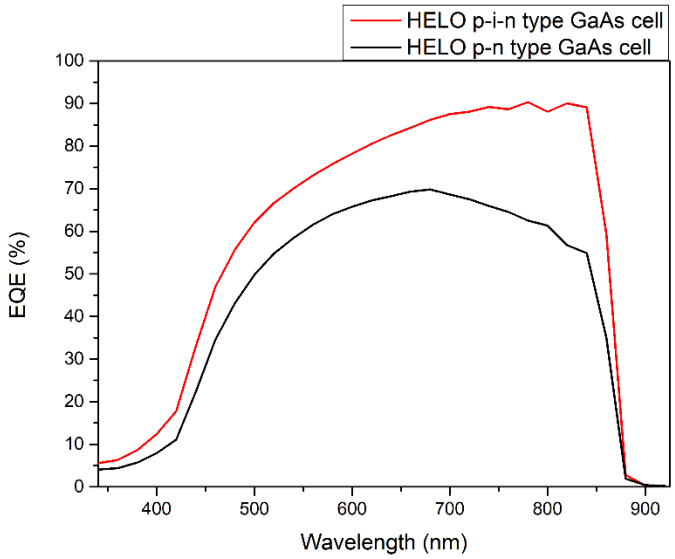

Figure 5.8. *Comparison of p-i-n type solar cells and p-n type solar cells*

Figure 5.9 comparatively shows quantum efficiency results of both reference ELO and HELO p-i-n GaAs cells. Both show similar behavior throughout the measured spectrum. The reference ELO solar cell is slightly better than HELO solar cell as expected. In comparison to ELO solar cells, the high density of dislocations within the HELO solar cell structure may have reduced carrier extraction. Nevertheless, this EQE result indicates that HELO solar cells have good crystal quality, thus good solar cell performance in terms of PCE can be expected. Integrated J_{sc} value of reference p-i-n type solar cell calculated as 23.21 mA/cm^2.

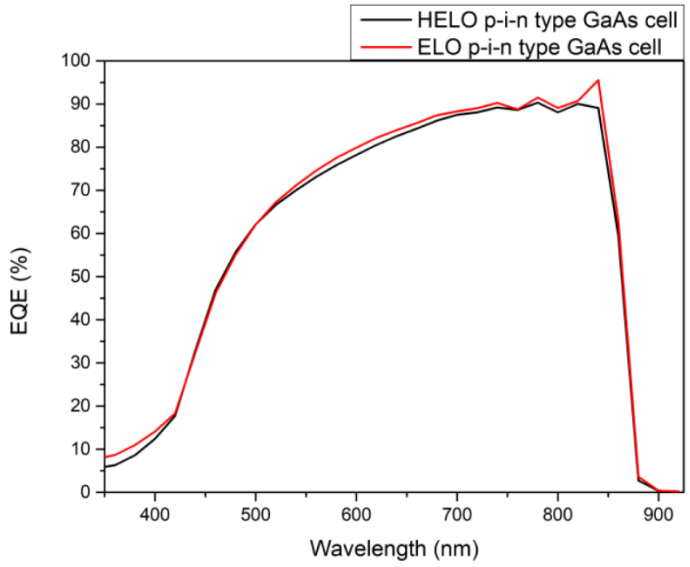

Figure 5.9. *Comparison of HELO and ELO GaAs cells*

Finally, Figure 5.10 shows the EQE performance comparison of ELO p-i-n type solar cells and ELO p-n type solar cells. The p-i-n type solar cells showed better EQE performance than the p-n type solar cells throughout the spectrum, particularly towards the back contact region. Despite being lower than p-i-n type solar cells, by being within the 70-80% band the p-n type solar cells demonstrated good performance for a solar cell.

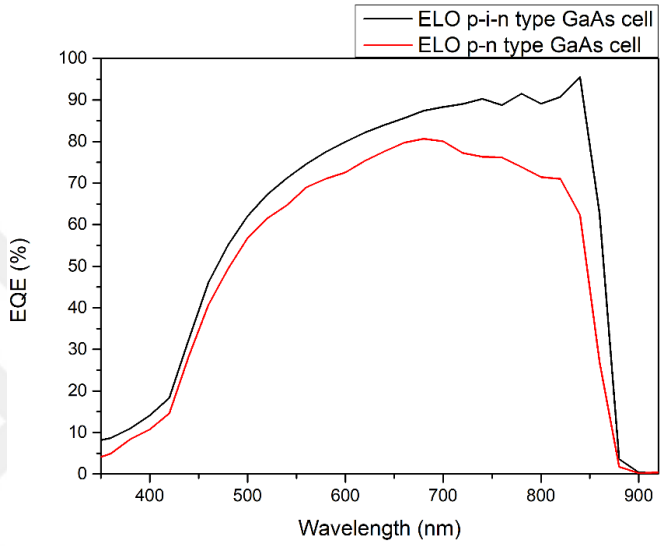

Figure 5.10. *EQE measurement comparison of p-i-n type and p-n type ELO cells*

5.5. Current-Voltage Measurement

Current-voltage (I-V) measurements were performed as the final step in determining the energy conversion and physical parameters of the solar cells. The J-V curve for ELO and HELO p-i-n solar cells is shown in Figure 5.11. The J_{sc} and V_{oc} of the ELO reference cell are 23.40 mA/cm^2 and 0.71 V, respectively. The J_{sc} and V_{oc} of the HELO cell, on the other hand, are 22.36 mA/cm^2 and 0.65 V, respectively. ELO and HELO GaAs cells were found to have PCE of 5.32% and 8.81%, respectively. The FF value of the ELO cell is 32% and the FF value of the HELO cell is 60.61%. The low conversion efficiency value of ELO reference solar cells is due to fabrication processes and resistances. Also, the low FF value of ELO reference solar cells indicates the high shunt and series resistance caused by the fabrication processes and poor flexible carrier surfaces. According to Figure 5.9, ELO reference solar cells must have had a higher

conversion efficiency value than the current value of it, around 20% PCE value could be expected.

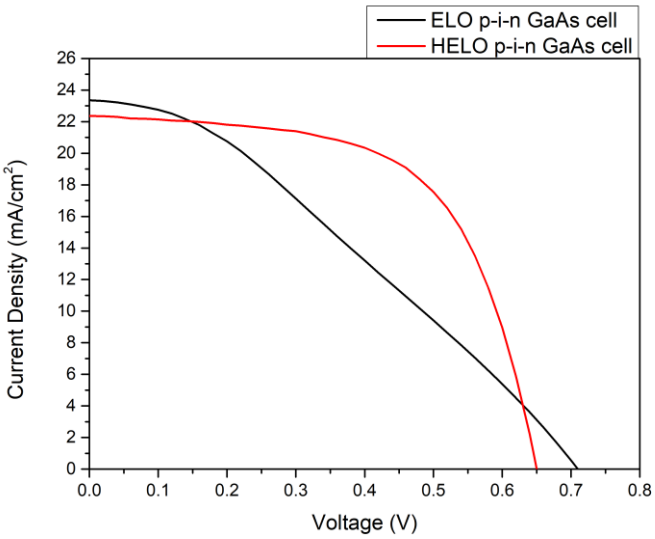

Figure 5.11. *J-V measurement of ELO and HELO p-i-n GaAs solar cells*

In Image 5.4, the surface of thin-film solar cells is given. Here, the rough surface morphology and lacerations can be seen. The roughness and laceration of thin-film polyamide surfaces are thought to be the biggest causes of poor device performance and shunt resistance. Polishing the polyamide surfaces or using smoother polyamides could improve the device's performance. With improvements in fabrication processes and using better flexible carriers, HELO GaAs solar cells with a conversion efficiency of 8.81% can be expected to reach the 15-20% band, even more can be expected for the ELO reference GaAs solar cells.

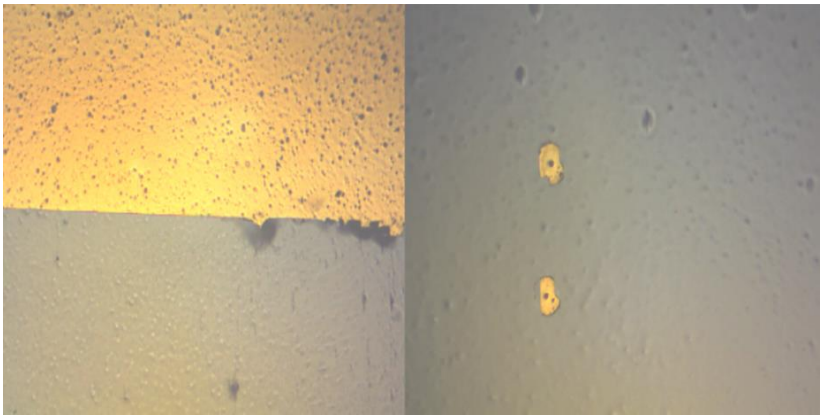

Image 5.4. *The surface of the thin-film solar cells*

Figure 5.12 depicts the comparison of HELO p-i-n solar cells and HELO p-n solar cells. The J_{sc} and V_{oc} of the HELO p-n GaAs solar cell are 18.55 mA/cm^2 and 0.515 V, respectively. The energy conversion efficiency of HELO p-n solar cells is found to be 4.52%. As previously stated, HELO p-n GaAs solar cells faced the same problems as other solar cells and had the potential to have a higher PCE than their current value.

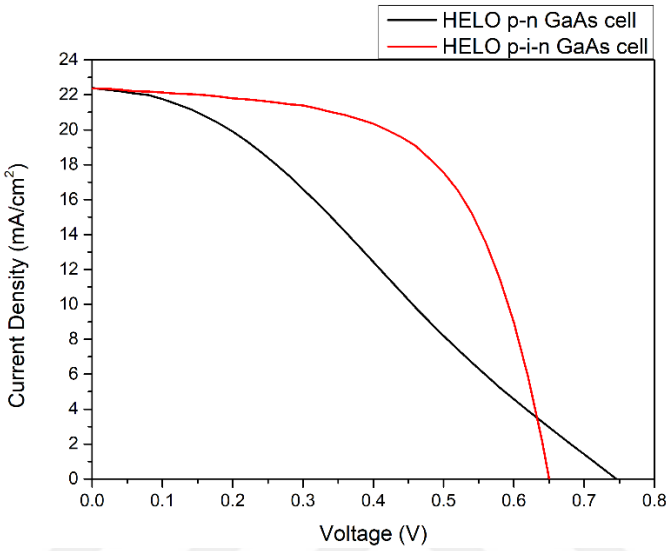

Figure 5.12. *J-V measurements of HELO p-i-n GaAs cells and HELO p-n GaAs cells*

Finally, Figure 5.13 shows the comparison of reference p-i-n GaAs solar cells and reference p-n GaAs solar cells. The J_{sc} and V_{oc} values of the ELO p-n GaAs solar cell were found as 27.81 mA/cm^2 and 0.864 V, respectively.

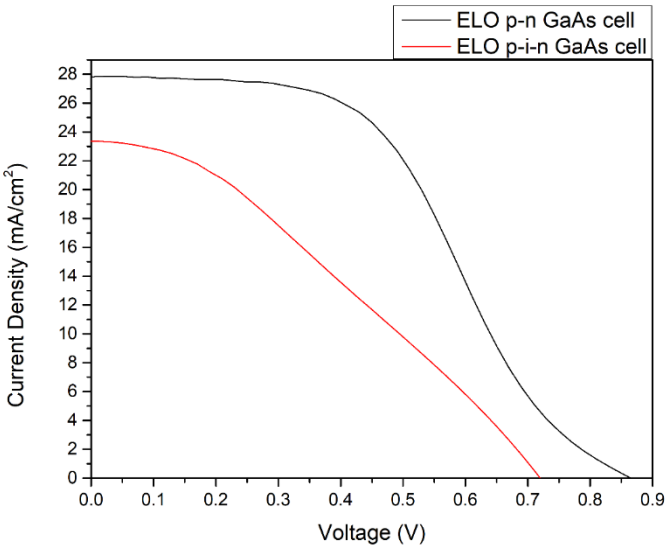

Figure 5.13. *J-V measurement comparison of ELO p-i-n GaAs cells and ELO p-n type GaAs cells*

The summary of calculated parameters from J-V measurements is given in Table 5.1.

Table 5.1. *A summary of main parameters of the HELO p-i-n, HELO p-n and ELO reference p-i-n solar cells under 1 sun AM1.5 spectrum*

Solar Cell	**Current Density (mA/cm^2)**	**Open Circuit Voltage (V)**	**Fill Factor (%)**	**Efficiency (%)**
p-i-n type HELO cell	22.36	0.65	60.61	8.81
p-i-n type ELO cell	23.40	0.71	32	5.32
p-n type HELO cell	18.55	0.515	47.34	4.52
p-n type ELO cell	27.81	0.864	46.21	11.10

6. CONCLUSION

III-V compounds are excellent materials for producing high-efficiency solar cells. The primary obstacle to large-scale solar cell applications for III-V compound materials is their high cost. Expensive III-V substrates account for nearly 90% of the overall cost of a solar cell in substrate-based solar cells. The main purpose of this thesis is to reduce the total cost of GaAs solar cells by employing Si substrates instead of expensive III-V substrates and to separate the active GaAs solar cell layer from its Si substrate using the epitaxial lift-off (ELO) process.

Thin-film GaAs solar cells are not only highly efficient but also lightweight and flexible, which is vital for space and military applications. Flexible and lightweight GaAs solar cells provide very high specific power (W/kg) and power density (W/m^2) with their high conversion efficiency. These features make them attractive for use in unmanned aircraft systems (UAS), high-altitude long-endurance (HALE) UAS, solar cell applications in space missions, mobile battery power for military uses, rooftop solar arrays etc.

When compared to III-V substrates, using Si wafer as a substrate offers low-cost and large-scale production. However, because of their different natures, the heteroepitaxial growth of GaAs on Si is challenging. The first difficulty was the formation of anti-phase domains (APDs) as a result of an apolar-polar mismatch. This problem can be overcome by employing 4° offcut Si substrates. Other difficulties include the difference in lattice and thermal expansion parameters between GaAs and Si. Misfit and threading dislocations are caused by lattice mismatch, whereas thermal mismatch creates microcracks in the device. They both have an adverse impact on solar cell performance. These difficulties can be minimized by employing various dislocation filter technologies and thermal annealing techniques. In this thesis, different approaches such as quantum dots (QD), strained superlattices (SLS), step-by-step AlGaAs/GaAs growth with thermal cycle annealing (TCA) were compared to obtain the highest quality crystals. The best results were obtained by employing 4° offcut Si substrates with step-by-step AlGaAs/GaAs growth in thermal cycle annealing. It was also observed that a single thin layer of the AlAs release layer operated as a dislocation filter, assisting in the reduction of defects in the active layer. The scanning electron microscopy (SEM), high-resolution X-ray diffraction (HRXRD), and photoluminescence (PL) techniques were used to make

the comparisons. After optimizing the parameters of crystal growth, an FWHM value of 150 arcsec band was achieved for the solar cells.

Following the selection of the dislocation filter approach, solar cells were grown as p-i-n type junction solar cells to compare the results from the p-n type junction solar cells. Measurements of external quantum efficiency (EQE) demonstrated that employing p-i-n type solar cells solved the problems of p-n type solar cells in the long-wavelength region. The spectral response of p-i-n type solar cells was in the 80-90% band in the range of 600-840 nm and performed approximately 20% better than p-n type solar cells within this spectrum. Furthermore, heteroepitaxial lifted-off (HELO) p-i-n solar cells performed as high as epitaxial lifted-off (ELO) reference p-i-n solar cells throughout the measured spectrum which indicates good crystal quality for the heteroepitaxial GaAs on Si solar cells.

In the final step, J-V measurements were taken to evaluate the performance of the solar cells. HELO p-i-n GaAs solar cells have achieved 8.81% efficiency at the AM1.5G spectrum, while HELO p-n GaAs solar cells have achieved 5.10%. The ELO reference p-i-n GaAs solar cells, on the other hand, has achieved 5.32% efficiency. This low-efficiency value of ELO reference cells relative to HELO p-i-n cells is caused by fabrication processes and roughness of the polyamide surfaces. Because the EQE values of both ELO and HELO p-i-n solar cells are good, higher efficiency values can be achieved. Improving fabrication processes and employing smoother polyamides would aid the efficiency of both solar cells.

With this work, previous results were improved and the highest efficiency of 8.81% has been achieved for the GaAs solar cells heteroepitaxial lifted-off from Si substrates. With the improvements to the fabrication processes, the power conversion efficiency of 15-20% band is achievable. First of all, better quality crystals are required to reduce threading dislocation densities (TDDs) in the solar cell. Therefore, the heteroepitaxy of GaAs on Si needs to be better understood and studied further. Second, a more effective window layer approach would improve the quantum efficiency of the high-energy photon region. AlGaAs were used as a window layer in the solar cells, and the Al ratio was kept low because Al could be affected by the ELO process. Due to the low Al ratio, AlGaAs used in solar cells gained the direct bandgap feature. This resulted in some absorption of high-energy photons at the front contact region, reducing the response of this region.

Third, the use of better and smoother polyamides would improve performance and prevent short-circuiting of solar cells. In the future, light trapping techniques to increase the optical path length within the solar cell or thinner solar cells to use the photon recycling effect could be used to improve performance.

REFERENCES

[1] Rabaia, M. K. H., Abdelkareem, M. A., Sayed, E. T., Elsaid, K., Chae, K.-J., Wilberforce, T., Olabi, A. G. (2020). Environmental impacts of solar energy systems: A review. *Science of The Total Environment*, 141989.

[2] http-1 : https://www.nrel.gov/pv/cell-efficiency.html

[3] Ward, J.S., Remo, T., Horowitz, K., Woodhouse, M., Sopori, B., VanSant, K., et al. (2016). Techno-economic analysis of three different substrate removal and reuse strategies for III-V solar cells. *Progress in Photovoltaics: Research and Applications*, 24 (9), 1284–1292.

[4] Yamaguchi, M., Ohmachi, Y., Oh'hara, T., Kadota, Y., Imaizumi, M., Matsuda, S. (2001). GaAs solar cells grown on Si substrates for space use. *Progress in Photovoltaics: Research and Applications*, 9(3), 191–201.

[5] Shockley, W. and Queisser, H.J. (1961). Detailed balance limit of efficiency of p-n junction solar cells. *Journal of Applied Physics*, 32 (3), 510–519.

[6] Green, M., Dunlop, E., Hohl-Ebinger, J., Yoshita, M., Kopidakis, N., and Hao, X. (2021). Solar cell efficiency tables (version 58). *Progress in Photovoltaics: Research and Applications*, 29 (7), 657-667.

[7] Wang, X., Wang, Z.M. (ed.), High-efficiency solar cells (2014), *Springer*, pp. 623-643.

[8] Horowitz, Kelsey A. W., Timothy Remo, Brittany Smith, and Aaron Ptak. (2018). Techno-Economic Analysis and Cost Reduction Roadmap for III-V Solar Cells. *Golden, CO: National Renewable Energy Laboratory*.

[9] Ding, H. and Sheng, X. (2019). Thin-film III-V single junction and multijunction solar cells and their integration onto heterogeneous substrates. *Inorganic Flexible Optoelectronics: Materials and Applications*, 177–208.

[10] Cappelluti, F., Ghione, G., Gioannini, M., Bauhuis, G., Mulder, P., Schermer, J., Liu, H. (2017). Novel Concepts for High-Efficiency Lightweight Space Solar Cells. *E3S Web of Conferences*, 16, 03007.

[11] Yablonovitch, E., Gmitter, T., Harbison, J. P. & Bhat, R. (1987). Extreme selectivity in the lift-off of epitaxial GaAs films. *Appl. Phys. Lett*. 51, 2222.

[12] Shahrjerdi, D. et al. (2012). High-efficiency thin-film InGaP/InGaAs/Ge tandem solar cells enabled by controlled spalling technology. *Appl. Phys. Lett*. 100, 3.

[13] McClelland, R. W., Bozler, C. O. & Fan, J. C. C. (1980). A technique for producing epitaxial films on reuseable substrates. *Appl. Phys. Lett*. 37, 560.

[14] Zahler, J. M. et al. (2007). High efficiency InGaAs solar cells on Si by InP layer transfer. *Appl. Phys. Lett.* 91, 012108.

[15] Bauhuis, G. J., Mulder, P., Schermer, J. J. (2013). Thin-Film III–V Solar Cells Using Epitaxial Lift-Off. *Springer Series in Materials Science*, 623–643.

[16] Konagai, M., Sugimoto, M., Takahashi, J. K. (1978). *Cryst. Growth*, 45, 277.

[17] Yablonovitch, E., Gmitter, T., Harbison, J. P. & Bhat, R. (1987). Extreme selectivity in the lift-offof epitaxial GaAs films. *Appl. Phys. Lett*., 51, 2222.

[18] Schermer, J. J., Bauhuis, G. J., Mulder, P., Meulemeesters, W. J., Haverkamp, E., Voncken, M. M. A. J., Larsen, P. K. (2000*). Appl. Phys. Lett*. 76, 2131.

[19] Bauhuis, G. J., Mulder, P., Haverkamp, E. J., Huijben, J. C. C. M. & Schermer, J. J. (2009). 26.1% thin-film GaAs solar cell using epitaxial lift-off. *Sol. Energy Mater. Sol. Cells*, 93, 1488–1491.

[20] Schermer, J. J. et al. (2006). Photon confinement in high-efficiency, thin-film III–V solar cells obtained by epitaxial lift-off. *Thin Solid Films*, 511-512, 645–653.

[21] Trautz, K., Jenkins, P., Walters, R., Scheiman, D., Hoheisel, R., Tatavarti, R., Osowski, M. (2013). High efficiency flexible solar panels. *2013 IEEE 39th Photovoltaic Specialists Conference (PVSC)*.

[22] Stender, C. L., Adams, J., Elarde, V., Major, T., Miyamoto, H., Osowski, M., Ragunathan, G. (2015). Flexible and lightweight epitaxial lift-off GaAs multi-junction solar cells for portable power and UAV applications. *2015 IEEE 42nd Photovoltaic Specialist Conference (PVSC).*

[23] http-2 : https://news.northropgrumman.com/news/features/northrop-grumman-technologies-support-nasas-insight-mars-lander

[24] http-3 : https://en.wikipedia.org/wiki/Solar_Impulse

[25] Li, J., Mastro, M., and Dadgar, A. (2011). III-V Compound semiconductors: integration with silicon-based microelectronics. *CRC Press.*

[26] Arpapay, B. (2019). Growth and characterization of group III-V nanostructures on Si substrates by MBE. *Eskisehir Technical University*. PhD Thesis.

[27] Aktas, M. (2020). Growth of GaAs epilayers on Si substrate for high efficiency thin film solar cell application. *Eskisehir Technical University.* MSc Thesis.

[28] Park, J.-S., Tang, M., Chen, S., & Liu, H. (2020). Heteroepitaxial Growth of III-V Semiconductors on Silicon. *Crystals*, 10(12), 1163.

[29] Wenham S. R., Green M.A., Watt M. E., Corkish R., Sproul A. (2011). Applied Photovoltaics. *Earthscan Publications Ltd.*

[30] Kasap, S. O. (2017). Principles of Electronic Materials and Devices. *McGraw Hill.*

[31] http-4 : https://pveducation.com

[32] Rahayu, F. (2015). HRXRD characterization of MBE epitaxial materials and related nanostructures. *Chalmers University of Technology*.

[33] Kaech, A. (2013). An introduction to electron microscopy instrumentation, imaging and preparation. Lecture Notes. *Center for microscopy and image analysis, University of Zurich.*

[34] Halmøy Wolden, E. (2015). Optical and electrical studies of GaAs nanowire arrays on Si substrates. *Norwegian University of Science and Technology*.

[35] Zaimler, H. (2019). Epitaxial lift-off of GaAs thin films and transferring on to the flexible carriers for solar cell applications, *Eskisehir technical University*. MSc Thesis.

[36] Arpapay, B. and Serincan, U. (2020). The role of antiphase domain boundary density on the surface roughness of GaSb epilayers grown on Si (001) substrates. *Superlattices and Microstructures*.

[37] Arpapay, B., Suyolcu, Y.E., Çorapçıoğlu, G., van Aken, P.A., Gülgün, M.A., and Serincan, U. (2020). A comparative study on {GaSb} epilayers grown on nominal and vicinal Si (100) substrates by molecular beam epitaxy. *Semiconductor Science and Technology,* 36 (2), 25011.

[38] Buyukpinar, A. (2021). Fabrication and characterization of thin-film GaAs solar cells peeled-off from Si substrates. *Eskisehir Technical University*. MSc Thesis.

[39] Kim, D.S., Jeong, Y., Jeong, H., and Jang, J.H. (2014). Triple-junction InGaP/GaAs/Ge solar cells integrated with polymethyl methacrylate subwavelength structure. *Applied Surface Science*, 320, 901–907.

[40] Klem, J. F., Jones, E. D., Myers, D. R., Lott, J. A. (1989). Characterization of thin AlGaAs/InGaAs/GaAs quantum-well structures bonded directly to SiO2/Si and glass substrates. *Journal of Applied Physics*, 66(1), 459–462.

[41] Fan, J. C., Lee, C. P., Tsai, C. M., Wang, S. Y., Tsang, J. S. (1998). Optical and structural properties of epitaxially lifted-off GaAs films. *Journal of Applied Physics*, 83(1), 466–468.

[42] Smets, A., Jäger, K., Isabella, O., van Swaaij, R., Zeman, R. (2015). Solar Energy: The physics and engineering of photovoltaic conversion technologies and systems. *UIT Cambridge, England.*

CURRICULUM VITAE

ORCID ID:

Name – Surname **:** Furkan Azim

Foreign Language **:** English

Education:

July 2019 – January 2022 **M.Sc.**

Eskisehir Technical University (ESTU)

Department of Physics

September 2016 – June 2019 **B.Sc.**

Eskisehir Technical University (ESTU)

Department of Physics

Experience:

January 2020 – January 2022 **ESTU Nanoboyut Research Laboratory**

M.Sc. Student

June 2019 – July 2019 **Akturk Research Group, Adnan Menderes University**

Intern